Evaluation of Eulerian multi-fluid versus Lagrangian methods for ejection of polydisperse evaporating sprays by vortices.

Stephane de Chaisemartin, Frédérique Laurent, Marc Massot, Julien Reveillon

Evaluation of Eulerian multi-fluid versus Lagrangian methods for ejection of polydisperse evaporating sprays by vortices

S. de Chaisemartin [a], F. Laurent [a], M. Massot [a,*], J. Reveillon [b]

[a] *EM2C-UPR CNRS 288, Laboratoire d'Energétique Macroscopique et Moléculaire Combustion, grande voie des vignes, 92295 Chatenay-Malabry, France*

[b] *CORIA-UMR CNRS 6614, Université de Rouen, site universitaire du Madrillet, 76801 Saint Etienne du Rouvray Cedex, France*

Abstract

The accurate simulation of the dynamics of polydisperse evaporating sprays in unsteady gaseous flows with large scale vortical structures is both a crucial issue for industrial applications and a challenge for modeling and scientific computing. The usual Lagrangian approaches developed in polydisperse unsteady configurations lead to a very high computational cost or to a low level of resolution if not enough numerical parcels are used. Besides, they induce coupling difficulties due to the different type of description of the two phases involved. A large range of Eulerian models have been recently developed to describe the disperse liquid phase with a lower cost and an easier coupling with a carrier gaseous phase. Among these models, the multi-fluid model allows the detailed description of polydispersity and size/velocity correlations of the droplets of various sizes. Such an approach has been shown to be derived from the Williams spray equation by Laurent and Massot [24] under the assumption of mono-kinetic spray number density functions conditioned by droplet size. Such an assumption is important since it defines the validity limit of the multi-fluid model and also results in the "pressureless gas dynamics" structure of the transport term in physical space of such a model. However, two key issues are still so far to be tackled : the validation in multi-dimensional configurations and the evaluation of the level of accuracy of such models versus the reference Lagrangian one as well as the related issue of a detailed study of the effective computational cost of the two approaches. In this work we study the impact of the mono-kinetic assumption in a multi-dimensional configuration at three levels : mathematical structure of the resulting system of conservation equations to be resolved in the multi-fluid model, numerical method needed to cope with the potential resulting singularities and physical interpretation and validity limit of the resulting numerical simulations. We then provide a sharp evaluation of the accuracy and computational cost of Eulerian models and related discretization schemes versus Lagrangian solvers in various unsteady configurations from Taylor-Green vortices to homogeneous isotropic turbulence.

Key words: Liquid Sprays, Polydispersity, Multi-fluid models, Spray equation, Presureless Gas Dynamics, Eulerian-Lagrangian comparisons.

1 Introduction

In many industrial combustion applications such as Diesel engines, fuel is stocked in condensed form and burned as a disperse liquid phase carried by a gaseous flow. Two phase effects as well as the polydisperse character of the droplet size distribution (since the droplets dynamics depend on their inertia and are conditioned by size) can significantly influence flame structures. Size distribution effects are also encountered in a crucial way in solid propellant rocket boosters, where the cloud of alumina particles experiences coalescence and becomes polydisperse in size, thus determining their global dynamical behavior [19, 20]. The coupling of dynamics, conditioned on particle size, with coalescence or aggregation as well as with evaporation can also be found in the study of fluidized beds [36, 15] and planet formation in solar nebulae. Consequently, it is important to have reliable models and numerical methods to be able to describe precisely the physics of two phase flows where the disperse phase is constituted of a cloud of particles of various sizes that can evaporate, coalesce or aggregate, break-up and also have their own inertia and size-conditioned dynamics. Since our main area of interest is combustion, we will work with sprays throughout this paper, keeping in mind the broad application fields related to this study.
By spray, we denote a disperse liquid phase (i.e. where the liquid volume fraction is much smaller than one) constituted of droplets carried by a gaseous phase. Even with this seemingly precise definition, two approaches corresponding to two levels of description can be distinguished. The first, associated with a full direct numerical simulation of the process, provides a model for the dynamics of the interface between the gas and liquid, as well as the exchanges of heat and mass between the two phases using various techniques such as the Volume Of Fluids (VOF) or Level Set methods (see for example [3, 18, 22, 35]). The second approach, based on a more global point of view thus called "mesoscopic", describes the droplets as a cloud of point particles for which the exchanges of mass, momentum and heat are described using a statistical point of view, with eventual correlations, and the details of the interface behavior, angular momentum of droplets, detailed internal temperature distribution inside the droplet, etc., are not predicted. Instead, a finite set of global properties such as size of spherical droplets, velocity of the center

* Corresponding author : M. Massot
Email address: marc.massot@em2c.ecp.fr (M. Massot).

of mass, temperature are modeled. Because it is the only one for which numerical simulations at the scale of a combustion chamber or in a free jet can be conducted, this "mesoscopic" point of view will be adopted in the present paper.

The principal physical processes that must be accounted for are (1) transport in real space, (2) droplet heating and evaporation, (3) acceleration of droplets due to drag, and (4) coalescence and break-up of droplets leading to polydispersity. Spray models have a common basis at the mesoscopic level (also called "the kinetic level" by analogy to the kinetic theory of gases [7, 8]), under the form of a number density function (NDF) satisfying a Boltzmann type equation, the so-called Williams [38, 39] equation. The internal variables characterizing one droplet are the size, the velocity and the temperature, so that the total phase space is usually high-dimensional. Such a transport equation describes the evolution of the NDF of the spray due to evaporation, to the drag force of the gaseous phase, to the heating of the droplets by the gas and finally to the droplet-droplet interactions, such as coalescence and break-up phenomena [14, 31, 2, 19, 24, 25].

There are several strategies in order to solve the liquid phase and the major challenge in numerical simulations is to account for the strong coupling between all the involved processes. A first choice is to approximate the NDF by a sample of discrete numerical parcels of particles of various sizes through a Lagrangian–Monte-Carlo approach [14, 31, 2, 19, 34]. It is called Direct Simulation Monte-Carlo method (DSMC) by Bird [4] and is generally considered to be the most accurate for solving Williams equation; it is especially suited for direct numerical simulations (DNS) since it does not introduce any numerical diffusion, the particle trajectories being exactly resolved. This approach has been widely used and it has been shown to be efficient in numerous cases (see for example [16] and references therein). Its main drawback, that was shown recently to be a major one with the development of new combustion chambers leading to combustion instabilities, is the coupling of an Eulerian description for the gaseous phase to a Lagrangian description of the disperse phase, thus offering limited possibilities of vectorization/parallelization and implicitation. Besides, it brings another difficulty associated with the repartition of the evaporated mass at the droplet location onto the Eulerian grid for the gas description. Moreover for unsteady computations of polydisperse sprays, a large number of parcels in each cell of the computational domain is generally needed, thus yielding large memory requirement and CPU cost.

This drawback makes the use of an Eulerian formulation for the description of the disperse phase attractive, at least as a complementary tool for Lagrangian solvers. It leads to the use of moments methods since the high dimension of the phase space prevents the use of DNS on the NDF equation with deterministic numerical methods like finite volumes. The use of moments methods leads to the loss of some information but the cost of such methods is usually much lower than the Lagrangian ones for two reasons. The first one is related to the fact that the number of unknowns we solve for is limited; the second

one is related to the high level of optimization one can reach when the two phases are both described by a Eulerian model.
However, the main drawbacks of most of the existing Eulerian models are their inability to capture the polydispersity in size of the spray as well as size-velocity correlations and the impossibility to treat droplet-droplet interactions because only a finite number of sizes are present in the problem. The introduction of presumed number density functions in size induces severe numerical instabilities mainly due to the fact that the evaporation process is not compatible with such a description and does not provide a satisfactory solution. The Eulerian Multi-Fluid model, extended by Laurent and Massot [24] from the ideas of Greenberg [17], allows to describe polydispersity of a spray in size and the associated size-conditionned dynamics. This approach relies on the derivation of a semi-kinetic model from the Williams equation using a moment method for velocity conditioned by droplet size, but keeping the continuous size distribution function [24]. This distribution function is then discretized using a "finite volume approach" in the size phase space that yields conservation equations for mass, momentum (and eventually other properties such as temperature) of droplets in fixed size intervals. This Multi-Fluid model is developed in the framework of a "Direct Numerical Simulation" for laminar flows, i.e. without modeled scales. However, it is symptomatic of the difficulties one will encounter in the development of Large Eddy Simulation tools for turbulent flows.

It is very often mentioned in the literature that Eulerian models lead to a computational cost which is much smaller than their Lagrangian counterpart. However, such a statement lacks precision for two reasons. First, the two methods do not resolve the same level of description, the Lagrangian approach providing a stochastic discretization of the "mesoscopic" Williams equation, whereas the Eulerian approach deals with a set of moments of the NDF. Thus to compare the two methods, we have to define precisely the configurations on which comparisons are relevant and then to investigate the accuracy of both methods in a such case (order of the method, numerical diffusion, convergence...). The selected configurations have also to be representative of the difficulties one will encounter in realistic devices : polydispersity and unsteadiness. Second, for a given level of accuracy and associated level of discretization, the computational efficiency of both methods have to be compared.

In order to be able to compare the accuracy of various numerical methods for the disperse phase, we restrict the simulation to one-way coupling and thus isolate the behavior of each method for a given gaseous flow. This, of course, does not prevent the use of the methods in the framework of two-way coupling, however we do not want to cope with the difficulties of two-way coupling and convergence of coupled Eulerian/Lagrangian solvers but solely to evaluate and compare two levels of description of the disperse liquid phase for given gaseous flows.

In the present work, we consider polydisperse evaporating sprays in large scale vortical structures of a gaseous field and we focus on the ejection process of the spray by the vortices in a one-way framework. Indeed it can be seen as an elementary process in turbulent dispersion of evaporating droplets, responsible for the segregation of droplets, a key issue for the global spray behavior [32]. Consequently precise modeling of this dynamics is a key point in describing more complex configurations. The objective of this paper is two-fold : first we present the ability of an Eulerian model to simulate accurately, for an evaporating polydisperse spray, the dynamics of ejection from vortices, and insist on the mathematical and numerical difficulties arising in multi-dimensional configurations. Indeed assumptions made at the kinetic level of modeling lead to a peculiar mathematical structure of the model, as far as transport in physical space is concerned, that can be related to the pressureless gas dynamics studied in [40, 5]. Elghobashi and Druzhinin in [11] noticed the peculiar structure of system of partial differential equations in the framework of bubbly flows and two-fluid modeling and proposed a Lagrangian-Eulerian mapping solver. However, they proposed a non-conservative scheme which can not handle the singularities created by finite Stokes droplets. We thus illustrate the formation of singularities created by the resulting conservation equations and define a critical Stokes number associated with it. As far as accuracy is concerned, we evaluate it comparing Eulerian and Lagrangian descriptions with a one-way coupling in configurations simple enough to perform precise quantitative comparisons. Both Eulerian and Lagrangian descriptions have been developed in two main configurations. The dynamics of ejection of evaporating droplets in a single vortex is accurately analyzed in the context of Taylor-Green vortices (a steady solution of inviscid Euler equations). We further investigate more complex configurations such as the dynamics of a polydisperse spray in an homogeneous and isotropic turbulent gaseous flow. Second, these comparisons allow an evaluation of the computational cost associated to each description. We can then evaluate the computational efficiency of both methods of resolution and characterize their behavior and limits in the various proposed configurations. To our knowledge, such an evaluation has not yet been conducted.

The paper is organized as follows. In section 2 the Williams spray equation is presented as well as the Lagrangian discretization and Eulerian multi-fluid modeling derived from it. The mathematical and numerical singularities arising in the Eulerian modeling are detailed in section 3 and the numerical method required to cope with them is explained in section 4. Finally we propose a detailed comparative study in the section 5 before concluding.

2 From mesoscopic to macroscopic spray modeling

2.1 Williams "kinetic" equation

In this section, we introduce a simplified Williams equation in the framework of our study. This mesoscopic approach is sometimes referred to as the "kinetic" level of description in reference to the kinetic theory of gases.

2.1.1 A simplified kinetic description

Let us define the NDF function f of the spray, where $f(t, \mathbf{x}, S, \mathbf{u})\mathrm{d}\mathbf{x}\mathrm{d}S\mathrm{d}\mathbf{u}$ denotes the averaged number of droplets (in a statistical sense), at time t, in a volume of size $\mathrm{d}\mathbf{x}$ around a space location $\mathbf{x}$, with a velocity in a $\mathrm{d}\mathbf{u}$-neighborhood of $\mathbf{u}$ and with a surface in a $\mathrm{d}S$-neighborhood of S. The droplets are considered to be spherical and characterized by their surface S.

For the sake of simplicity and for the purpose of this paper, we are going to consider that the evaporation process is described by a d^2 law without convective corrections and that the drag force is given by a Stokes law. We also assume that the spray is dilute enough to neglect the droplet interactions, and finally that the unstationary heating of the droplets does not need to be modeled so that the evaporation law coefficient does not depend on the heating status of the droplet. We refer to [1, 24, 25] for more detailed droplet models for which the derivation of the multi-fluid model can be easily extended. The extension of the multi-fluid model to more detailed droplet models does not have an impact on the conclusions of the present study; it is established that refined droplet models can be used as long as they do not include history terms (see [24, 25]).

Concerning the gaseous phase, its temperature and composition are assumed to be constant and uniform as well as its main physical properties such as mass density and viscosity. The evaporation process modifies the composition of the gas phase and can eventually lead to its saturation in regions of large droplet density. However, we do not attempt to achieve a fully coupled calculation, but only to evaluate the accuracy of the Eulerian multi-fluid model relatively to the Lagrangian solver, as well as to study the compared computational cost of the two approaches for the spray descriptions. We are thus assuming a one-way coupling between the carrier gaseous phase and the disperse liquid phase. The evolution of the spray is then described by the Williams transport equation [38] :

$$\partial_t f + \mathbf{u} \cdot \partial_{\mathbf{x}} f + \partial_S(K\, f) + \partial_{\mathbf{u}} \cdot (\mathbf{F}\, f) = 0 \tag{1}$$

where K denotes the d^2 law evaporation rate, which is constant because of the assumptions on the gaseous field. $\mathbf{F}$ is the Stokes drag force due to the velocity difference with the gaseous phase. This quantity has the following dependence : $\mathbf{F} = \mathbf{F}(t, \mathbf{x}, \mathbf{u}, S)$; the dependence on the local gas velocity is implicitly written in the $(t, \mathbf{x})$ dependence :

$$\mathbf{F}(t, \mathbf{x}, \mathbf{u}, S) = \frac{\mathbf{U}(t, \mathbf{x}) - \mathbf{u}}{\tau_p(S)}, \qquad \tau_p(S) = \frac{\rho_l S}{18\pi\mu_g}, \tag{2}$$

where $\mathbf{U}$ is the gas velocity, μ_g represents its dynamic viscosity and ρ_l is the liquid density. Note that the dynamical viscosity and the liquid density are assumed to be constant.

2.1.2 Non dimensional numbers

We introduce here a non dimensional form of the kinetic equation used in the following, highlighting the non dimensional numbers of the problem.

$$\partial_{t^*} f^* + \partial_{\mathbf{x}^*} \cdot (\mathbf{u}^*\, f^*) + -\mathrm{E_v}\, \partial_{S^*} f^* + \partial_{\mathbf{u}^*} \cdot \left(\frac{\mathbf{U}^* - \mathbf{u}^*}{\mathrm{St}(S^*)} f^* \right) = 0. \tag{3}$$

We use characteristic quantities of the gaseous phase, a spatial length λ, a velocity A and the corresponding time $\tau_g = \lambda/A$, to define the non dimensional quantities. We also define a characteristic size S_{ref} being chosen for example as the maximal droplet surface of the distribution. The dimensionless variables are then defined by :

$$t^* = \frac{t}{\tau_g},\ \mathbf{x}^* = \frac{\mathbf{x}}{\lambda},\ \mathbf{u}^* = \frac{\mathbf{u}}{A},\ \mathbf{U}^* = \frac{\mathbf{U}}{A},\ S^* = \frac{S}{S_{ref}}, \tag{4}$$

and $f^*(t^*, \mathbf{x}^*, \mathbf{u}^*, S^*) = f(t, \mathbf{x}, \mathbf{u}, S)\lambda^3 A^3 S_{ref}$ is the distribution function corresponding to this change of variables. This operation leads to the outbreak of two non dimensional numbers, driving the physics of the problem. The first one is the Stokes number, defined by $\mathrm{St} = \tau_p(S_{ref})/\tau_g$, where τ_p is the dynamical time of the droplets of size S_{ref} defined by Eq. (2). The second non dimensional number outbreaking in Eq. (3) is $\mathrm{E_v}$. It is defined as the ratio between the characteristic time of the gaseous flow τ_g and the characteristic time of the evaporation process τ_{evap} :

$$\mathrm{E_v} = \frac{\tau_g}{\tau_{evap}}, \qquad \tau_{evap} = \frac{S_{ref}}{-K}. \tag{5}$$

This non dimensional number will drive the evaporation speed of the droplets in the computations.

In the following, we will have to work with mass densities of droplets with a size between two limits $[S_{k-1}, S_k[$, where the full droplet size interval is $[0, S_{ref}]$.

Consequently, we will introduce the non-dimensional mass densities by :

$$m^{*(k)} = \lambda^3 \frac{m^{(k)}}{M_{ref}} = \int_{S^*_{k-1}}^{S^*_k} S^{*3/2} f^*(S^*)\, dS^*, \tag{6}$$

where M_{ref} is the characteristic mass associated to the reference droplet surface S_{ref} :

$$M_{ref} = \frac{\rho_l S_{ref}^{3/2}}{6\sqrt{\pi}}, \qquad S^*_k = S_k / S_{ref}. \tag{7}$$

Since we will work with only non-dimensional quantities throughout the paper, from now on, for the sake of legibility, we will drop the stars and keep in mind that all the variables are non-dimensional.

2.2 Lagrangian and Eulerian modeling

We present the Lagrangian Monte-Carlo treatment of this modeling and then recall the main steps of the derivation of the Eulerian multi-fluid model from the kinetic Williams-Boltzmann equation. The complete details of the derivation can be found in [24]. The idea is here to obtain the multi-fluid's equations highlighting their interest in describing a polydisperse evaporating spray.

2.2.1 Lagrangian method

To solve the kinetic equation of the spray, we can use Lagrangian Monte-Carlo methods. This leads to Euler-Lagrange numerical methods, commonly used for the calculation of polydisperse sprays in various application fields (see for example [31, 20, 29, 30, 34, 32] and references therein). In this kind of approach, the gas phase is generally computed using a deterministic Eulerian solver, while the disperse phase is treated in a Lagrangian way. The influence of the droplets on the gas flow is taken into account by the presence of source terms in the system of gas conservation equations. However, as explained in the previous section, this influence is outside of the scope of this paper.

Two Lagrangian methods can then be used for the disperse phase depending on the level at which the physical processes are modeled. But these methods are equivalent in our case, in a sense which will be specified. The first one is a Discrete Particle Simulation (DPS), which describes the evolution of numerical particles, each one representing one or several droplets. The physical processes such as transport, evaporation, drag force are then described by the classical following equations :

$$d_t \mathbf{x}_k = \mathbf{u}_k, \quad d_t \mathbf{u}_k = \frac{\mathbf{U}(t, \mathbf{x}_k) - \mathbf{u}_k}{\mathrm{St}(S_k)}, \quad d_t S_k = -E_v, \tag{8}$$

where, $\mathbf{x}_k$ is the non-dimensional position of the k^{th} numerical particle, $\mathbf{u}_k$ its non-dimensional velocity and S_k its non-dimensional surface. The Eulerian fields for the liquid phase are usually recovered through ensemble averages [33].

The second Lagrangian method is a Particle Discretization (PD) of the Williams governing equation given with non-dimensional variables by Eq. (3). The distribution is then written as a sum of Dirac delta functions :

$$f(t, \mathbf{u}, S) = \sum_k w_k \delta(\mathbf{x} - \mathbf{x}_k(t)) \delta(\mathbf{u} - \mathbf{u}_k(t)) \delta(S - S_k(t)). \tag{9}$$

where w_k is the constant weight of the k^{th} numerical particle and $\mathbf{x}_k$, $\mathbf{u}_k$, S_k are its position, velocity and surface. These characteristics of numerical particles evolve through the Eqs. (8). This method provides directly an ensemble average of the droplet repartition and then the Eulerian fields. This point of view is different from the previous one since we use directly a statistical description of the spray, coherently to what is done with the Eulerian method. However, the two Lagrangian methods are equivalent in our case without any droplet interaction because physical processes are all linear in the droplet number. Indeed, doing several realizations of the DPS (saying with the same number of particles for each) is the same as doing one simulation with the PD method putting together all the particles of all the realizations of the DPS. Conversely, doing a simulation with the PD method is the same as doing a number N of realizations of DPS, with initially a number Nw_k of particles having the characteristics $\mathbf{x}_k$, $\mathbf{u}_k$ and S_k, N being an integer such that each Nw_k is an integer. The cost of the two kinds of simulations is then about the same and the main difference between these two methods comes from their initialization; it can be seen from what precedes that the second one generally leads to a smaller number of total numerical particles for the same level of accuracy. As a conclusion, since the statistical description of the spray is coherent with the Eulerian method used for the liquid phase and since it leads to less costly computations, the second Lagrangian method is used here. Eqs. (8) are solved using a third order explicit Runge-Kutta method. Moreover, as already mentioned, the initialization process is crucial, since it defines the number of numerical particles and has to be a realization of the initial distribution. We assume that the droplet size spectrum of the spray is independent of the space location at the initial time. Since the physically relevant global variable to be considered is the droplet mass density, we take the initial mass distribution $f_0(x, y, S)$ in the form :

$$f_0(x, y, S) = m_0^{\text{tot}} \frac{S^{3/2} f_s(S)}{\int\limits_{[0,1]} \sigma^{3/2} f_s(\sigma) d\sigma} \frac{f_{xy}(x, y)}{\int\limits_{[0,1]^2} f_{xy}(x', y') \mathrm{d}x' \mathrm{d}y'} \tag{10}$$

where m_0^{tot} is the total non-dimensional mass density of the spray, $f_s(S)$ is the size distribution function given in Figure 3 and the space distribution f_{xy}

is identically equal to 1 in the uniform case and is represented in Figure 8 for the non uniform configuration. The initialization can be done in several ways : simulating a uniform distribution on the support of f_0 and adjusting the weights to obtain the correct distribution is easy but it induces particles with a very small mass density and thus little efficiency in terms of computational cost. A better method consists in simulating directly the mass distribution through a reject method with numerical particles having weights representing the same mass density. Since our global initial mass distribution f_0 is bounded by a constant C times the probability density function of the uniform law on $\Omega \times [0,1]$, where $\Omega \subset [0,1] \times [0,1]$ is the space where droplets can be found, initial conditions can be obtained in the following way : four random numbers (X_k, Y_k, S_k, U_k) between 0 and 1 are chosen; if $\mathbf{x}_k = (X_k, Y_k)$ belongs to Ω and if $f_0(\mathbf{x}_k, S_i) > CU_k$, then the particle is accepted; if not, it is rejected. This is done till the number N of accepted numerical particles we want is reached. Then, each numerical particle (X_k, Y_k, S_k) has the weight $\omega_k = m_0^{\text{tot}}/(NS_k^{3/2})$.

For comparisons purposes with the Eulerian method, some averages are done on space cells C_α and sections $[S_{m-1}, S_m]$ in droplet size to find the approximation of the corresponding non-dimensional mass density $m_{\alpha,m}^{La}$ and velocities $\mathbf{u}_{\alpha,m}^{La}$:

$$m_{\alpha,m}^{La} = \sum w_k S_k^{3/2}, \quad m_{\alpha,m}^{La}\mathbf{u}_{\alpha,m}^{La} = \sum w_k S_k^{3/2}\mathbf{u}_k \tag{11}$$

where the summation is done over all k such that $S_{m-1} \leq S_k < S_m$ and $\mathbf{x}_k \in C_\alpha$. The accuracy of such ensemble averages is discussed in the following.

2.2.2 Eulerian multi-fluid model

The formalism and the associated assumptions needed to derive the Eulerian multi-fluid model are introduced in [24]. We recall briefly here the main steps.

Two steps are to be realized in order to obtain the Eulerian multi-fluid model's equations. In a first step we reduce the size of the phase space, considering only the moments of order zero and one in the velocity variable at a given time, a given position and for a given droplet size : $n = \int f \mathrm{d}\mathbf{u}$ and $\bar{\mathbf{u}} = \int \mathbf{u} f \mathrm{d}\mathbf{u}/n$ which depend on $(t, \mathbf{x}, S)$. The closure of the system is obtained through the following assumptions :

[H1] For a given droplet size, at a given point $(t, \mathbf{x})$, there is only one characteristic averaged velocity $\bar{\mathbf{u}}(t, \mathbf{x}, S)$.

[H2] The velocity dispersion around the averaged velocity $\overline{u}(t, \mathbf{x}, S)$ is zero in each direction, whatever the point $(t, \mathbf{x}, S)$.

It is equivalent to presume the following NDF conditioned by droplet size :

$$f(t, \mathbf{x}, S, \mathbf{u}) = n(t, \mathbf{x}, S)\delta(\mathbf{u} - \bar{\mathbf{u}}(t, \mathbf{x}, S)), \tag{12}$$

that is to reduce the support of the NDF to a one dimensional submanifold parametrized by droplet size.

Such an assumption leads to a closed system of conservation equations called the semi-kinetic model on the moments of order zero and one in velocity. It is given by two partial differential equations in the variables $n(t, \mathbf{x}, S)$ and $\bar{\mathbf{u}}(t, \mathbf{x}, S)$ which express the conservation of the number density of droplets and their momentum, respectively, at a given location $\mathbf{x}$ and for a given size S :

$$\partial_t n + \partial_{\mathbf{x}} \cdot (n\overline{\mathbf{u}}) - \mathrm{E_v}\partial_S(n) = 0. \tag{13}$$

$$\partial_t(n\,\overline{\mathbf{u}}) + \partial_{\mathbf{x}} \cdot (n\,\overline{\mathbf{u}} \otimes \overline{\mathbf{u}}) - \mathrm{E_v}\partial_S(n\,\overline{\mathbf{u}}) - n\overline{\mathbf{F}} = 0, \tag{14}$$

where $\overline{\mathbf{F}}(t, \mathbf{x}, S)$ is the Stokes's drag force taken at $\mathbf{u} = \overline{\mathbf{u}}$. It has to be noticed that the two descriptions at the "kinetic" level and at the moment level are equivalent as long as (i) the assumption that the NDF conditioned by droplet size is mono-kinetic, i.e. satisfies Eq. (12) and associate one single velocity at a fixed position and time for a given droplet size, and (ii) the solution of the system of conservation equations remains smooth. Such a model can also be interpreted as a one node DQMOM approach on the NDF, where n is its weight and $\mathbf{u}$ its abscissa [27]. The validity of such and assumption and its limitations are fully discussed in the following.

The second step consists in choosing a discretization $0 = S_0 < S_1 < \cdots < S_N$ for the droplet size phase space and to average the obtained system of conservation laws over each fixed size intervals $[S_{k-1}, S_k[$, called section. The set of droplets in one section can be seen as a "fluid" for which conservation equations are written. The sections exchange mass and momentum. To close the system, the following assumptions are introduced :

[H3] In one section, the characteristic averaged velocity do not depend on the size of the droplets.

[H4] The form of n as a function of S is supposed to be independent of t and $\mathbf{x}$ in a given section, thus decoupling the evolution of the mass concentration of droplets in a section from the repartition in terms of sizes.

These assumptions are equivalent to presume the NDF in size and in velocity inside each section :

$$\begin{cases} \forall S \in [S_{k-1}, S_k[\quad n(t, \mathbf{x}, S) = m^{(k)}(t, \mathbf{x})\kappa^{(k)}(S) \\ \text{and} \quad \bar{\mathbf{u}}(t, x, S) = \bar{\mathbf{u}}^{(k)}(t, \mathbf{x}), \end{cases} \tag{15}$$

where $m^{(k)}$ is the mass concentration of droplets in the k^{th} section, in such a way that

$$\int_{S_{k-1}}^{S_k} S^{3/2}\kappa^{(k)}(S)\mathrm{d}S = 1. \tag{16}$$

It is interesting to note that such an approach only focuses on one moment of order 3/2 of the distribution in the size variable inside one section. This moment corresponds to the mass density of droplets and is the only one to be transported and conserved; it has been chosen because of its relevance to the evaporation and combustion processes. The conservation equations for the k^{th} section then read :

$$\begin{aligned}
\partial_t m^{(k)} + \partial_x \cdot (m^{(k)} \bar{\mathbf{u}}^{(k)}) &= -\mathrm{E_v}\,(E_1^{(k)} + E_2^{(k)}) m^{(k)} \\
&\quad +\mathrm{E_v}\, E_1^{(k+1)} m^{(k+1)}, \\
\partial_t (m^{(k)} \bar{\mathbf{u}}^{(k)}) + \partial_x \cdot (m^{(k)} \bar{\mathbf{u}}^{(k)} \otimes \bar{\mathbf{u}}^{(k)}) &= -\mathrm{E_v}\,(E_1^{(k)} + E_2^{(k)}) m^{(k)} \bar{\mathbf{u}}^{(k)} \\
&\quad +\mathrm{E_v}\, E_1^{(k+1)} m^{(k+1)} \bar{\mathbf{u}}^{(k+1)} + m^{(k)} \bar{\mathbf{F}}^{(k)},
\end{aligned} \tag{17}$$

where $E_1^{(k)}$ and $E_2^{(k)}$ are the "classical" pre-calculated evaporation coefficients :

$$E_1^{(k)} = S_{k-1}^{3/2} \kappa^{(k)}(S_{k-1}), \quad E_2^{(k)} = \frac{3}{2} \int_{S_{k-1}}^{S_k} S^{1/2} \kappa^{(k)}(S) \mathrm{d}S, \tag{18}$$

where $\mathbf{F}^{(k)}$ is the "classical" averaged drag force [17, 24] :

$$\bar{\mathbf{F}}^{(k)} = \frac{\mathbf{U} - \bar{\mathbf{u}}^{(k)}}{\mathrm{St}_{\mathrm{mean}}^{(k)}}, \quad \frac{1}{\mathrm{St}_{\mathrm{mean}}^{(k)}} = \int_{S_{k-1}}^{S_k} \frac{S^{3/2}\, \kappa^{(k)}(S)}{\mathrm{St}(S)} \mathrm{d}S. \tag{19}$$

As specified in [24] the terms with $E_1^{(k)}$ and $E_2^{(k)}$ represent the exchange terms between successive sections and exchange terms with the gaseous phase, respectively. These conservation equations have, as far as physical transport is concerned, a peculiar structure similar to those of the pressureless gas dynamics. They lead to singular behaviors requiring well-adapted numerical methods, as it will be presented in the next section.

3 Mathematical structure and development of singularities

The assumptions formulated at the kinetic and at the macroscopic level while deriving the Eulerian model, lead to several mathematical difficulties. Indeed we obtain a peculiar system of conservation equations without any pressure term leading to singularities called "δ-shocks". These singularities occur when the mono-kinetic assumption of the multi-fluid model ceases to be valid and introduces some artificial velocity averaging. The key issue is thus to characterize the appearance of such singularities and to relate it to the physics of droplet dynamics. This will have two consequences, first we will be able to choose comparison configurations which are within the validity limit of the

multi-fluid model; second, since the configurations of interest frequently involve flow location which can be a little beyond the validity limit and still can be accurately described by the multi-fluid model, we aim at developing a numerical method robust enough to cope with these singularities in case they do occur.

3.1 Mathematical peculiarities of Multi-fluid modeling

This multi-fluid system of equations contains a peculiar transport term similar to the pressureless gas system studied for example in [5]. Indeed, it is similar to an Euler gas dynamics system of equations, but without any pressure term in the momentum equation; that is, it corresponds to the limit of zero temperature :

$$\begin{aligned} \partial_t(\rho) + \partial_{\mathbf{x}} \cdot (\rho \bar{\mathbf{u}}) &= 0, & (20) \\ \partial_t(\rho \bar{\mathbf{u}}) + \partial_{\mathbf{x}} \cdot (\rho \bar{\mathbf{u}} \otimes \bar{\mathbf{u}}) &= 0. & (21) \end{aligned}$$

This system can be found for example in astrophysics, when describing the formation of large scale structures in the universe or in the modeling of sticky particles [40]; it has also been presented in [11] for bubbles. It has the peculiarity to be weakly hyperbolic and can generate "δ-shocks" (that is a discontinuity in velocity which leads to Dirac delta function concentration in density) or create vacuum zones. Note that it is important to be able to cope efficiently with vacuum zones since they represent areas of the flow where no droplet is to be found and are commonly encountered in most applications. In fact the equation on the velocity itself is decoupled from the conservation of mass and takes the form of the Burger's classical equation :

$$\partial_t \mathbf{u} + \mathbf{u} \cdot \partial_x \mathbf{u} = 0. \quad (22)$$

A shock may then arise, leading to the concentration of density at its interface. This shock occurs for example when droplets cross each-other : indeed we have at the same space and time location two velocities. In the resolution of the whole problem, as formulated in Eq. 17, the drag term will decrease the occurrence of such crossings, attracting droplet velocity towards gas velocity. Nevertheless, for droplets inertial enough, influence of drag is weaker and crossings may still occur. As we already mentioned in the assumption [H1], section 2.2.2, we only have one averaged velocity at a given point, preventing the description of droplet crossings. In the two-fluid model, also based on one averaged velocity, the same problem occurs and droplet crossings can neither be described. However, in the multi-fluid model, as presented in assumption [H1], we have one averaged velocity at a given size. Consequently, the polydispersity described in the multi-fluid model allows crossing of droplets pro-

vided they do not belong to the same size interval. Nevertheless, equally-sized droplet crossings are out of the limits of the multi-fluid model and can not be described.

This observation has two consequences. First we want to be able to control droplet dynamics for a given gaseous flow. Indeed for turbulent flows or even for laminar flows with contra-rotative vortices or impinging jets, equally-sized droplet crossings may occur. We would like to be able, through a limitation on the Stokes number of the droplets, to foresee these crossings and to prevent them to occur. Second we want to develop a numerical method robust enough to cope with the velocity discontinuities and density concentration arising if equally-sized droplet crossings do still occur at rare occasions in the flow.

A specific numerical method is consequently needed, requiring :

- to stand high gradients even up to the situation where all the mass density would be concentrated in one cell;
- to preserve the positivity of mass density;
- to reproduce a discrete maximum principle on the velocity.

Furthermore, we also want an order of accuracy high enough in cases of regular distribution to limit the number of cells needed, in order to treat multi-dimensional configurations. The development of such a numerical method is presented in section 4.

3.2 Detailed analysis of multi-fluid limits

The peculiar structure of the multi-fluid system and the set of associated assumptions require a precise analysis of droplet dynamics description. The purpose of this section is to provide the key ideas of the analysis yielding the definition of a critical Stokes number below which the assumptions of the multi-fluid are valid. We first introduce the fundamentals of the analysis in a typical one dimensional problem defining the critical Stokes number. We then extend this definition to two-dimensional problems in the context of Taylor-Green vortices for the gaseous flow. The extension to a more general framework for more complex flow field is then considered. Finally we perform Lagrangian numerical applications in these configurations, to study the validity of the theoretical criterion introduced.

3.2.1 1-D model problem and critical Stokes number

The purpose of the present section is to identify the critical point for the appearance of "δ-shocks" [5, 6], that is, the eventual concentration up to infinity

of the density field related to the creation of a discontinuous velocity field. Such an event corresponds to the crossing of characteristic curves in the physical space [26] and to the limit of the mono-kinetic character of the NDF at the kinetic level, i.e. the velocity distribution at given location becomes multi-valued. These characteristic curves are defined, for both the kinetic equation (3) and the system of conservation laws (13,14), in the case of non-evaporating droplets, by a set of ordinary differential equations (ODE) and initial conditions :

$$\begin{cases} \mathrm{d}_t X_p = V_p \\ \mathrm{d}_t V_p = \dfrac{U(t,X_p) - V_p}{\mathrm{St}} \end{cases}, \quad \begin{cases} X_p(0) = X_p^0 \\ V_p(0) = V_p^0 \end{cases}, \tag{23}$$

with $V_p^0 = u^0(X_p^0)$ since the initial distribution is mono-kinetic. It should be noticed that the non-linear coupling between the two fields is contained in the fact that the gaseous velocity field U is only sampled by the droplet trajectory at X_p. Thus, the characteristic curves are the integral curves of the vector field defined by (23), parametrized by the initial spatial coordinate so that we will adopt the notation $(X_p, V_p)^t(t, X_p^0)$. Under some standard conditions on the regularity of the field U, the characteristic curves exist and are well-defined for all time and spatial initial conditions. However, as soon as some characteristic curves cross each other in the only spatial projection of the characteristic diagram (x, t), the distribution ceases to be mono-kinetic and the equivalence between the macroscopic and kinetic descriptions is not valid any more. In fact the characteristics never cross each other in the (x, v) phase space so that the distribution admits multiple velocities at a point where the spatial projection of the characteristics cross each-other. For the sake of simplicity the generic example of steady gaseous flow field is given by a spatial harmonic oscillation $U(x) = \sin(2\pi\, x)$, with periodic boundary condition on the spatial interval $[0, 1]$. The initial condition for the spray is a uniform zero velocity distribution $u^0 = 0$, as well as a constant density distribution $n^0 = 1$. The characteristic first crossing point can be shown to be at $x = 1/2$ since this is the point of maximal strain. In order to characterize the limit we linearize the original system of ODEs (23) at $x = 1/2$ for which the eigenvalues of the associated matrix are real, if and only if $8\pi\,\mathrm{St} \leq 1$. The limiting value of the Stokes number is then $1/(8\pi) \approx 0.0398$. Taking a look at Figure 1 will provide the reader with the intuitive picture of two cases where there is or is not characteristic crossing. We have represented on the left the trajectories of the particles (that are also the characteristic curves in this pressureless configuration) with the usual convention that the abscissa is the spatial coordinate and the ordinate, the time evolution. We consider thirty equidistributed initial spatial positions and a zero initial velocity. We plotted the evolution of the position versus time for two Stokes numbers which are below and above the critical one. It can be clearly seen that the characteristics cross at $x = 0.5$ for $\mathrm{St} = 0.3$ at time around $t = 0.5$ which corresponds to the first time when the velocity distribution at $x = 0.5$ becomes multi-valued as shown in the

position-velocity phase plane on the top-right of Figure 1. On the contrary, such a scenario never occurs for St = 0.03 for which the characteristic curves never cross and the velocity field as a function of position always remain mono-kinetic as presented in Figure 1-bottom.

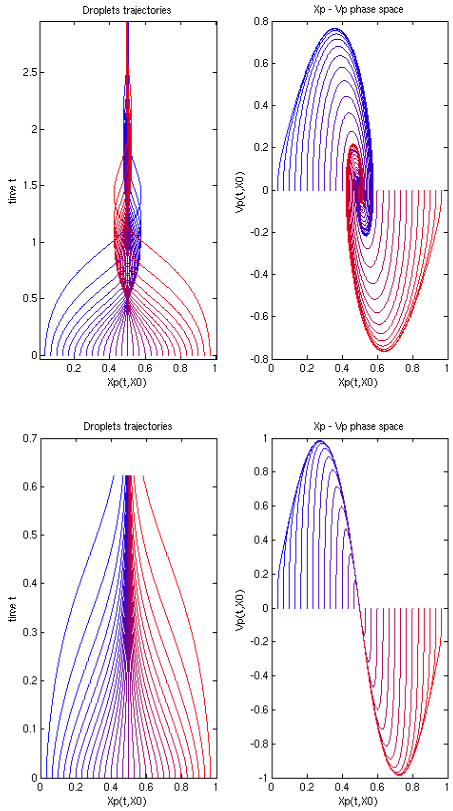

Fig. 1. (top) : St = 0.3, characteristic crossing in the (x, t) plane (left) and phase plane dynamics (x, v) (right) for 30 initial conditions equally distributed in space with zero initial velocity; (bottom) : St = 0.03, no characteristic crossing in the (x, t) plane (left) and phase plane dynamics (x, v) (right) for 30 initial conditions equally distributed in space with zero initial velocity.

Besides, as shown in [12] in the 1D case, the droplet velocity field is rapidly attracted, within a non dimensional time equal to a few Stokes number, to an invariant velocity manifold. It is smooth only if the non-dimensional Stokes number is below the critical limit and becomes discontinuous beyond this threshold, thus allowing the droplets to go from one half of the domain to the other (see Figure 1-top for St = 0.3). This manifold is easily observed in the (X_p, V_p) phase plane in Figure 1-top-right for $\mathrm{St} = 0.03 < 1/(8\pi)$.

For Stokes numbers beyond the critical limit, let us underline the fact that, even for the Williams equation at the kinetic level, there is a singularity at the time when the characteristics are crossing in the (x, t) diagram. At this exact time, the zeroth order moment of the NDF, that is the number density of

droplets, becomes infinite at $x = 1/2$ and the original modeling at the kinetic level can cease to be valid if the initial droplet number density is high enough for the collision term to become important in the neighborhood of the axis of symmetry where the singularity occurs. Even if this singularity is spatially integrable, the original modeling on the NDF should then involve a collision term or a "granular pressure". For an interesting study of the influence of the initial number density of droplets on the influence of the collisional term in the NDF equation in a different framework, we refer to the work of Volkov and collaborators (see [37] and references therein).

This will prove to be symptomatic of what happens in multi-dimensional configurations with more complex flows.

3.2.2 Taylor-Green vortices

In a first step toward more complex multi-dimensional configurations, we investigate a gaseous flow field which is given by the two-dimensional Taylor Green vortices, a steady solution of the inviscid incompressible Euler equations. The reason for such a choice is related to the fact that while being two-dimensional, such a configuration is representative of the vortical structure of turbulent flows and still allows an analytical treatment that will highlights the study of more complex configurations. To extend the study to a two-dimensional version of the steady spatially oscillating gaseous flow field, we consider a steady solution of the incompressible Euler equations with periodic boundary conditions, which reads in the non-dimensional setting $U = \sin(2\,\pi\,x)\,\cos(2\,\pi\,y)$ for the horizontal velocity, and $V = -\cos(2\,\pi\,x)\,\sin(2\,\pi\,y)$ for the vertical one, $(x, y) \in [0, 1] \times [0, 1]$. The structure of the flow field is presented in Figure 2 through the velocity vectors.

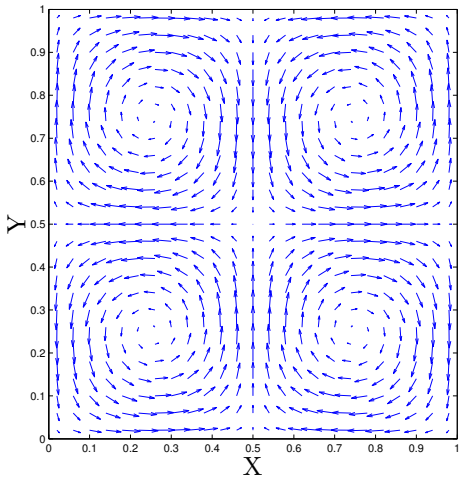

Fig. 2. Velocity vectors of Taylor-Green gaseous vortices configuration.

In order to analytically characterize the critical Stokes number, we focus on the behavior of the system around the central point $(1/2, 1/2)$. The characteristics, in their non-dimensional form, are then linearized at this point and it yields :

$$\begin{cases} \mathrm{d}_t X_p = U_p, \ \mathrm{d}_t U_p \ = \dfrac{2\,\pi\, X_p - U_p}{\mathrm{St}}, \\ \\ \mathrm{d}_t Y_p \ = V_p, \ \ \mathrm{d}_t V_p \ = \dfrac{-2\,\pi\, Y_p - V_p}{\mathrm{St}}. \end{cases} \tag{24}$$

The system of four ODEs can then be splitted into two decoupled system of ODEs in each direction which can be treated separately. In the x direction, the eigenvalues are always real, whereas, in the y direction, we recover the same analysis as in the 1D case, with the same critical value of the Stokes number. It can be shown that, for the considered initial mono-kinetic velocity distribution, the first point of characterics crossing is at the center : $(1/2, 1/2)$ which is again the point of maximum rate of strain.

Beyond the obtained Stokes critical value, droplets are ejected from vortices and encounter droplets coming from other vortices, since the original number density of droplets is symmetrical. Consequently, for Stokes numbers below this critical value, we are sure that the multi-fluid assumptions are valid in the sense that the kinetic modeling and the fluid modeling provide identical descriptions. For Stokes numbers beyond this critical value, the multi-fluid model and the kinetic model provide diverging solutions and are not equivalent any more. The Eulerian semi-kinetic and multi-fluid models both lead to infinite density concentrations and discontinuous velocity fields. In fact, in the non-dimensional gas velocity variables, the maximal value of the strain for both 1D and 2D cases is 2π at the symmetry point.

To obtain a first numerical illustration of the previously introduced Stokes criteria, we perform Lagrangian simulations in this Taylor-Green configuration to study droplets dynamics evolution with their inertia. The analytical velocity field allows us to compute analytically the gas velocity at the position of the droplets. We decided to introduce in the computational domain a uniform distribution of droplets, equally distributed in the domain. Concerning the distribution in the size phase space, we have a polydisperse distribution reproducing $f^0(S)$ represented in Figure 3. This droplet size distribution does not depend on spatial coordinate. We choose two maximum Stokes numbers for this distribution : a Stokes number under the critical value $\mathrm{St} = 0.03 < \mathrm{St}_c$ and one over the critical value $\mathrm{St} = 0.3 > \mathrm{St}_c$. Results are represented at four different times in Figure 4 and Figure 5. As expected, the droplets with a Stokes number under the critical value are ejected from the gaseous vortices, and they accumulate at the edges of the vortices without leaving their original vortex, see Figure 4. On the contrary, more inertial droplets with a Stokes number over the critical value are ejected from their original vortex leading to

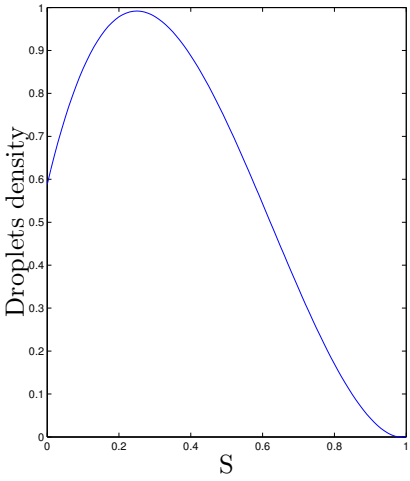

Fig. 3. Initial conditions for droplets : non-dimensional polydisperse size distribution.

crossing trajectories for droplets as shown in Figure 5.

3.2.3 Extension to a general framework

The purpose of this subsection is to illustrate what happens in the framework of a more complex gaseous velocity field and to point out the similarities with what has just been presented in the context of Taylor-Green vortices.

In the previous study, we have considered only zero initial droplet velocity distribution and conducted a study of the critical Stokes number in terms of the gaseous flow field. In fact, in a general framework, there is also a condition on the initial droplet velocity field. From [21] it can be shown that system (13,14) is equivalent to the kinetic Williams equation for mono-kinetic initial velocity distributions under two conditions on both the initial velocity field $\overline{\mathbf{u}}^0$ and on the maximum $a^{\max}$ of the derivative of the steady gaseous velocity field. The variable $a^{\max}$ denotes the maximal rate of strain of the gaseous flow field. In non-dimensional variables, the conditions can be written $a^{\max}\,\mathrm{St} < 1/(4\,d)$ and $|\partial_{\mathbf{x}}\overline{\mathbf{u}}^0|_\infty\,\mathrm{St} < 1/(2\,d)$, d being the number of dimension of the physical space. Since in the preceding case, $a^{\max} = 2\,\pi$, one recovers the obtained condition on the critical Stokes number in the one-dimensional setting. These two conditions insure, from a mathematical point of view, that the kinetic NDF will remain mono-kinetic, if it was originally so, for all times. In this context this provides a rigorous basis to insure the validity of the semi-kinetic and multi-fluid model.

We can thus tackle the configuration of a given non-dimensional gaseous flow field. The point we want to make is related to the previous study, and relates to a new set of non-dimensional values of (x^0, a^0) for which a typical "eddy

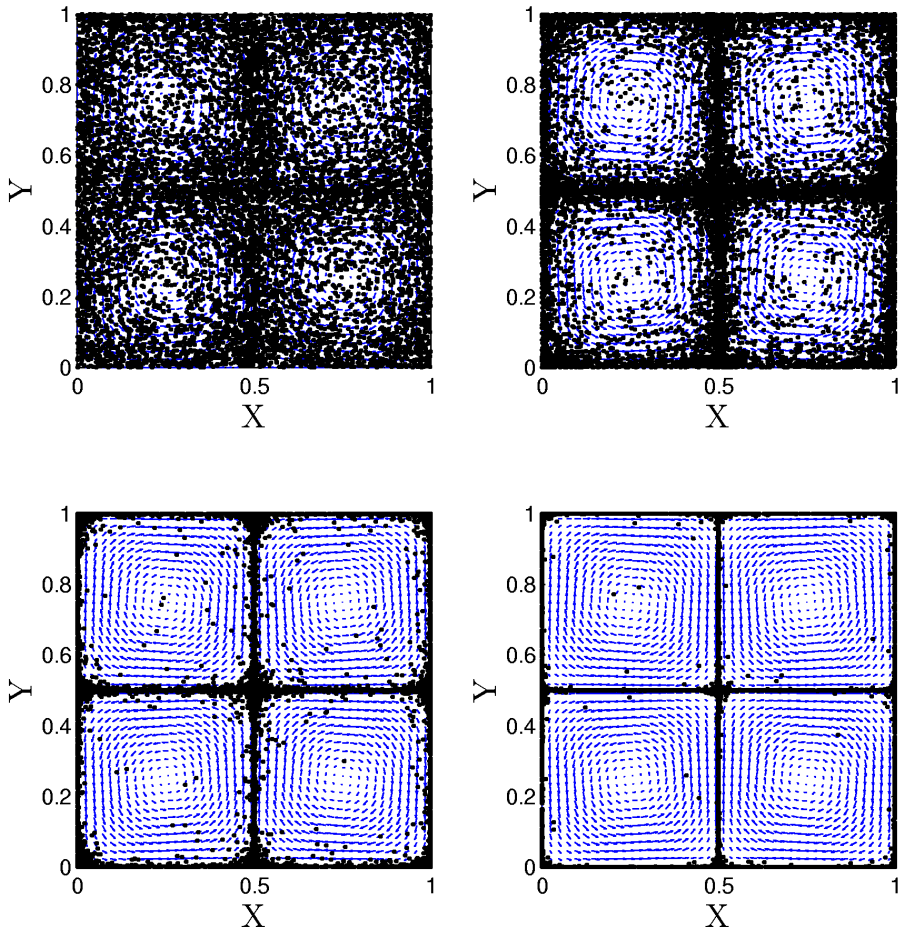

Fig. 4. Lagrangian numerical parcels position at time $t = 0.5$, $t = 1.25$, $t = 2.75$, and $t = 4$ in the non dimensional setting. Positions are plotted over velocity vectors of the gaseous Taylor-Green vortices. The maximum Stokes number of the droplets distribution is $\mathrm{St} = 0.03 < \mathrm{St}_c$. Computation with 10000 numerical parcels.

size" in the new space variable $x^+ = x/x^0$ and a related typical "rate of strain" in the new velocity variable $U^+ = U/(x^0\, a^0)$ are respectively one. In this framework, using the previous result, we will define the critical new Stokes number St_c^+ as being $1/4$, which will yield the original critical Stokes Number $\mathrm{St}_c = 1/(4\, a^0)$.

The only point remaining to be fulfilled is the choice of the couple (x^0, a^0). In the Taylor Green vortices, this choice is obvious, since the typical vortex size is $x^0 = 1$ and the typical rate of strain is $a^0 = 2\pi$, thus yielding the obtained value $\mathrm{St}_c = 1/8\pi$.

As long as the flow is incompressible, the two eigenvalues of the symmetric

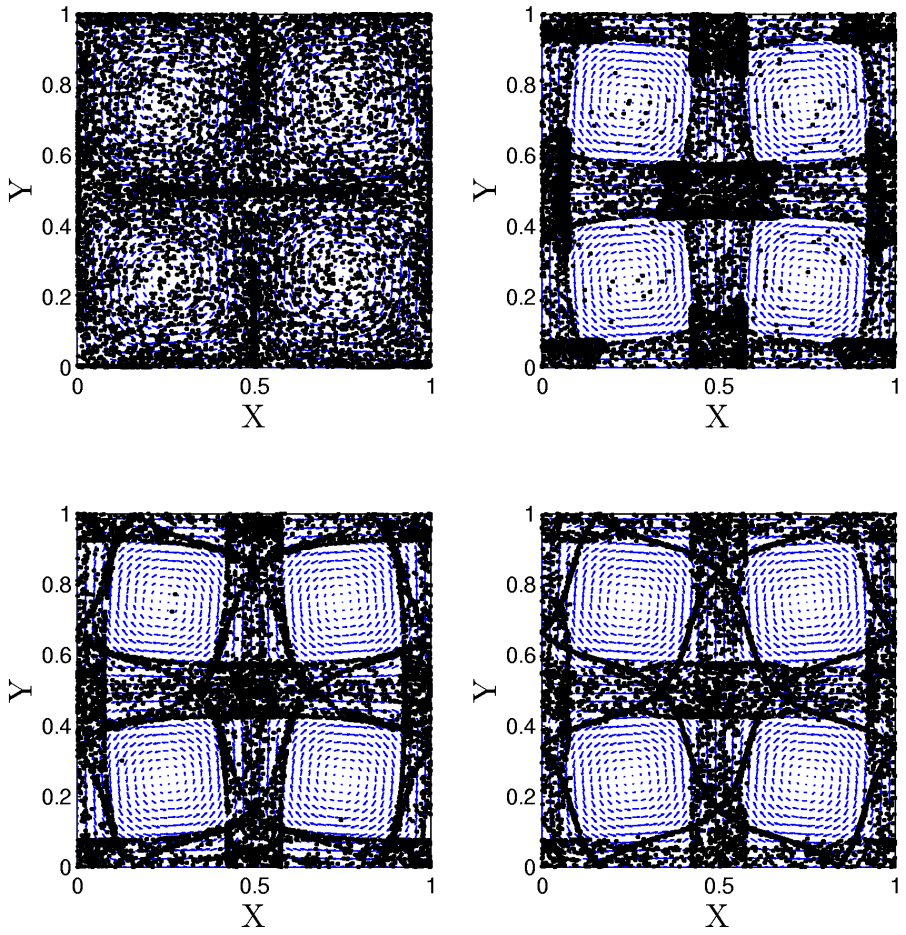

Fig. 5. Lagrangian numerical parcels position at time $t = 0.5$, $t = 1.25$, $t = 2.75$, and $t = 4$ in the non dimensional setting. The positions are plotted over velocity vectors of the gaseous Taylor-Green vortices. The maximum Stokes number of the droplets distribution is $\mathrm{St} = 0.3 > \mathrm{St}_c$. Computation with 10000 numerical parcels.

part of the velocity tensor are of opposite sign and the positive eigenvalue is then presented. More precisely :

$$\partial_{x,y} \begin{bmatrix} U \\ V \end{bmatrix} = \begin{bmatrix} \partial_x U & \dfrac{\partial_y U + \partial_x V}{2} \\ \dfrac{\partial_y U + \partial_x V}{2} & \partial_y V \end{bmatrix} + \frac{\omega}{2} \begin{bmatrix} 0 & 1 \\ -1 & 0 \end{bmatrix} \tag{25}$$

where $\omega = \partial_y U - \partial_x V$ is the vorticity field and $\pm i\omega/2$ are the two eigenvalues of the second matrix. The eigenvalues of the first matrix read :

$$\lambda_\pm = \frac{1}{2}\left(\partial_x U + \partial_y V \pm \sqrt{f(U,V)}\right) \tag{26}$$

with :

$$f(U,V) = (\partial_x U - \partial_y V)^2 + (\partial_y U + \partial_x V)^2 \tag{27}$$

For the case of study of an incompressible velocity field in 2D, the zero-divergence of the flow imposes that there are two opposite eigenvalues. A characteristic value of a_0 can then be determined from the field of λ_+, from the distribution of this eigenvalue in the flow field. We can then determine the corresponding critical Stokes number : $\mathrm{St}_c = 1/(4\,a_0)$. Such definition will be used in section 4.5.3, in the case of a turbulent gaseous flow field.

4 Eulerian multi-fluid specific numerical method

The mathematical and numerical issues tackled in the previous subsection require the development of a specific numerical method able to cope with potentially developing singularities.

4.1 General Scheme

Phenomena involved in our problem are of two different types : transport induces an evolution in the physical space without leading to any interaction between the sections, whereas transport in internal coordinate space, i.e. size and velocity through evaporation and drag, induces an evolution without any coupling with the spatial coordinates. It is then interesting to separate them through a splitting algorithm. We choose a Strang splitting which is second order in time provided all the steps are second order in time, with the following structure : (see [10])

- Evaporation and drag force during $\Delta t/2$
- Transport during Δt
- Evaporation and drag force during $\Delta t/2$

This approach has the great advantage to preserve the properties of the schemes we use for the different contributions, as for example maximum principle or positivity. If we assume that the involved phenomena evolve at roughly similar time scales, this Strang splitting algorithm guaranties a second order precision in time provided that each of the elementary schemes has a second order time precision. Furthermore, in the case of the simple modeling used for the purpose of this paper, we can decouple evaporation and drag force and treat them separately in the splitting algorithm.

4.2 Drag term

To present the drag force treatment, we focus only on this term and recall the different steps from the kinetic level to the multi-fluid model. We recall our choice of a Stokes drag force at the kinetic level, leading to a simple relaxation of the liquid velocity to the gas velocity with a characteristic number St :

$$\partial_t f + \partial_{\mathbf{u}} \left(\frac{\mathbf{U}(t) - \mathbf{u}}{\mathrm{St}(S)} f \right) = 0. \tag{28}$$

The next step is, as before, to obtain the semi-kinetic system of equations :

$$\begin{cases} d_t n &= 0, \\ d_t(n\mathbf{u}) &= n \dfrac{\mathbf{U}(t) - \mathbf{u}}{\mathrm{St}(S)}. \end{cases} \tag{29}$$

And, with the assumption that the velocity is constant inside a section, the moments of order 3/2 on the surface over the k^{th} section lead to the system :

$$\begin{cases} d_t m^{(k)} &= 0, \\ d_t(m^{(k)} \bar{\mathbf{u}}^{(k)}) &= m^{(k)} \dfrac{\mathbf{U}(t) - \bar{\mathbf{u}}^{(k)}}{\mathrm{St}(S_u^k)}, \end{cases} \tag{30}$$

where the mean surface S_u^k only depends on the choice of the distribution's shape $\kappa^{(k)}$ in the k^{th} section; it reads here :

$$S_u^k = \frac{3}{5} \frac{S_k^{5/2} - S_{k-1}^{5/2}}{S_k^{3/2} - S_{k-1}^{3/2}}. \tag{31}$$

The system (30) is solved exactly for a stationary gas velocity, insuring a good accuracy in time and leading to the scheme :

$$\begin{aligned} m^{(k)}(t_{n+1}) &= m^{(k)}(t_n) \\ \bar{\mathbf{u}}^{(k)}(t_{n+1}) &= \mathbf{U} + (\bar{\mathbf{u}}^{(k)}(t_n) - \mathbf{U}) \exp\left(-\frac{\Delta t}{\mathrm{St}(S_u^k)} \right). \end{aligned} \tag{32}$$

The order of precision of the splitting step solving evaporation and drag force will thus depend on the order of the evaporation method.

4.3 Evaporation method

To present the numerical method used to solve the evaporation term, we recall here the system of equations focusing only on this evaporation term :

$$
\begin{aligned}
d_t(m^{(k)}) &= -\mathrm{E_v}\,(E_1^{(k)} + E_2^{(k)})m^{(k)} + \mathrm{E_v}\,E_1^{(k+1)}m^{(k+1)},\\
d_t(m^{(k)}\overline{\mathbf{u}}^{(k)}) &= -\mathrm{E_v}\,(E_1^{(k)} + E_2^{(k)})m^{(k)}\overline{\mathbf{u}}^{(k)} + \mathrm{E_v}\,E_1^{(k+1)}m^{(k+1)}\overline{\mathbf{u}}^{(k+1)}.
\end{aligned}
\tag{33}
$$

Furthermore, as presented in the assumptions to derive the multi-fluid model, we have to choose a form $\kappa^{(k)}(S)$ of the distribution in the k^{th} section (see Eq. 15). Here, this function is chosen constant since it is the optimal choice for it, as shown in [23]. The expressions of $\kappa^{(k)}$, $E_1^{(k)}$ and $E_2^{(k)}$ are given by :

$$
\kappa^{(k)} = \frac{5}{2(S_k^{5/2} - S_{k-1}^{5/2})},
\tag{34}
$$

and

$$
E_1^{(k)} = \frac{5S_{k-1}^{3/2}}{2(S_k^{5/2} - S_{k-1}^{5/2})}, \quad E_2^{(k)} = \frac{5(S_k^{3/2} - S_{k-1}^{3/2})}{2(S_k^{5/2} - S_{k-1}^{5/2})}.
\tag{35}
$$

The finite volumes discretization recalled here is proved to be a first order method in [23]. We need then to perform a time discretization to solve the multi-fluid system of equations : we have chosen a θ-scheme, with $\theta = 1/2$. This scheme offers unconditional stability, preserves the positivity of the mass density in each section and is second order accurate in time. It is a semi-implicit scheme, but, with a constant time step, it can be written $(\mathbb{I} + \frac{\Delta t}{2}C)U^{n+1} = (\mathbb{I} - \frac{\Delta t}{2}C)U^n$ with U^n the vector of the mass densities of the sections at time t_n or the vector of momentum of the sections at time t_n. Besides, $\mathbb{I}$ is the identity matrix and C is a bidiagonal matrix, independent of n, which has the coefficients $E_1^{(k)} + E_2^{(k)}$ on the diagonal and $-E_1^{(k)}$ on the upper-diagonal.

4.4 Kinetic transport scheme

Bouchut et al. developed in [6] a second order kinetic schemes, which is a finite volume scheme based on the equivalence between a macroscopic and a microscopic level of description for the pressureless gas equations :

$$
\partial_t f + u\partial_x f = 0 \iff \begin{cases} \partial_t(\rho) + \partial_x \cdot (\rho\overline{u}) = 0 \\ \partial_t(\rho\overline{u}) + \partial_x \cdot (\rho\overline{u} \otimes \overline{u}) = 0 \end{cases}
\tag{36}
$$

with :

$$
f(t,x,u) = \rho(t,x)\delta(u - \overline{u}(t,x)).
\tag{37}
$$

The values of ρ and $\overline{u}$ are then recovered from f by the formula :

$$
\begin{pmatrix} \rho \\ \overline{u} \end{pmatrix}(t,x) = \int_{\mathbb{R}} \begin{pmatrix} 1 \\ u \end{pmatrix} f(t,x,u)\mathrm{d}u.
\tag{38}
$$

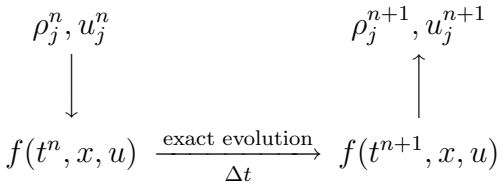

Fig. 6. Main steps of the kinetic based transport scheme

The principle of such method is illustrated in figure Fig. 6 for the 1D case. It is a volume finite method giving approximations ρ_j^n and $q_j^n = \rho_j^n u_j^n$ of the following averaged values on each cell $[x_{j-1/2}, x_{j+1/2}]$ of ρ and ρu at each discrete time t^n :

$$\rho_j^n \simeq \frac{1}{\Delta x} \int_{x_{j-1/2}}^{x_{j+1/2}} \rho(t^n, x) \mathrm{d}x \tag{39}$$

$$q_j^n = \rho_j^n u_j^n \simeq \frac{1}{\Delta x} \int_{x_{j-1/2}}^{x_{j+1/2}} \rho(t^n, x) \overline{u}(t^n, x) \mathrm{d}x. \tag{40}$$

First, at time $t = t^n$, a distribution function $f^n(x, u)$ is reconstructed from the averaged values ρ_j^n and q_j^n. This comes from Eq. (37) and, for example, a piecewise linear reconstruction of $\rho(t^n, x)$ and $\overline{u}(t^n, x)$ with adequate slope limiters. Second, the kinetic equation is solved analytically between t^n and t^{n+1} : $f(t, x, u) = f^n(x - u(t - t^n), u)$. Finally, a projection of $f(t^{n+1-}, x, u)$ is done to find ρ_j^{n+1} and q_j^{n+1}, which corresponds to the average on each cell of (38) at $t = t^{n+1-}$. This leads to the following scheme :

$$\rho_j^{n+1} = \rho_j^n - \frac{\Delta t}{\Delta x}(F_{j+1/2}^{(1)} - F_{j-1/2}^{(1)}) \tag{41}$$

$$q_j^{n+1} = q_j^n - \frac{\Delta t}{\Delta x}(F_{j+1/2}^{(2)} - F_{j-1/2}^{(2)}) \tag{42}$$

with the fluxes :

$$F_{j+1/2} = \begin{pmatrix} F_{j+1/2}^{(1)} \\ F_{j+1/2}^{(2)} \end{pmatrix} = \frac{1}{\Delta t} \int_{t^n}^{t^{n+1}} \int_{\mathbb{R}} \begin{pmatrix} 1 \\ u \end{pmatrix} u\, f^n(x_{trans}, u) \mathrm{d}u \mathrm{d}t. \tag{43}$$

and with

$$x_{trans} = x_{j+1/2} - u(t - t^n). \tag{44}$$

The obtained fluxes rely, through Eq. (37), on the reconstructions of $\rho^n(x) = \rho(t^n, x)$ and $\overline{u}^n(x) = \overline{u}(t^n, x)$ from the discrete values ρ_j^n and u_j^n. Different type of reconstructions are proposed in [6]. We choose the one that gives good results without being too complex : a piecewise linear reconstruction. The

functions $\rho^n(x)$ and $\overline{u}^n(x)$ are then written, for x between $x_{j-1/2}$ and $x_{j+1/2}$:

$$\begin{cases} \rho^n(x) = \rho_j^n + D\rho_j^n(x - x_j), \\ \overline{u}^n(x) = \overline{u}_j^n + Du_j^n(x - x_j), \end{cases} \tag{45}$$

with

$$\overline{u}_j^n = u_j^n - \frac{D\rho_j^n Du_j^n}{12\rho_j^n}(\Delta x)^2, \tag{46}$$

in order to conserve the momentum. The slope $D\rho_j^n$ is obtain here using a MC limiter to limit the numerical diffusion, which is different to what is done in [6] where a minmod limiter was used :

$$D\rho_j^n = \begin{cases} \min\left(2\frac{\rho_{j+1}^n - \rho_j^n}{\Delta x}, 2\frac{\rho_j^n - \rho_{j-1}^n}{\Delta x}, \frac{\rho_{j+1}^n - \rho_{j-1}^n}{2\Delta x}\right) & \text{if } \rho_{j-1}^n < \rho_j^n < \rho_{j+1}^n \\ \max\left(2\frac{\rho_{j+1}^n - \rho_j^n}{\Delta x}, 2\frac{\rho_j^n - \rho_{j-1}^n}{\Delta x}, \frac{\rho_{j+1}^n - \rho_{j-1}^n}{2\Delta x}\right) & \text{if } \rho_{j-1}^n > \rho_j^n > \rho_{j+1}^n \\ 0 & \text{otherwise} \end{cases} \tag{47}$$

The slope Du_j^n is chosen in order to guarantee the maximum principle property on the velocity and also the CFL like condition :

$$\begin{aligned} Du_j^n = & \frac{1}{2}\left(\mathrm{sgn}(u_{j+1}^n - u_j^n) + \mathrm{sgn}(u_j^n - u_{j-1}^n)\right) \\ & \times \min\left\{\frac{|u_{j+1}^n - u_j^n|}{(1 - \Delta x D\rho_j^n/6\rho_j^n)\Delta x}, \frac{|u_j^n - u_{j-1}^n|}{(1 + \Delta x D\rho_j^n/6\rho_j^n)\Delta x}, \frac{1}{\Delta t}\right\}. \end{aligned} \tag{48}$$

Let us denotes ρ_j^I, ρ_j^{II}, u_j^I, u_j^{II} the corresponding values of $\rho^n(x)$ and $\overline{u}^n(x)$ at the bounds $x_{j-1/2}$ and $x_{j+1/2}$ of the j^{th} cell. The fluxes are then given by : $F_{j-1/2}^{(1)} = F_{j-1/2}^{+(1)} + F_{j-1/2}^{-(1)}$, $F_{j-1/2}^{(2)} = F_{j-1/2}^{+(2)} + F_{j-1/2}^{-(2)}$ and

$$\begin{aligned} F_{j+1/2}^{+(1)} &= \frac{\rho_j^{II}(u_j^{II})_+}{1 + \Delta t D u_j^n} - \frac{\Delta t}{2} D\rho_j^n \frac{u_j^{II}(u_j^{II})_+}{(1 + \Delta t D u_j^n)^2}, \\ F_{j-1/2}^{-(1)} &= \frac{\rho_j^{I}(u_j^{I})_-}{1 + \Delta t D u_j^n} - \frac{\Delta t}{2} D\rho_j^n \frac{u_j^{I}(u_j^{I})_-}{(1 + \Delta t D u_j^n)^2}, \\ F_{j+1/2}^{+(2)} &= \rho_j^{II} u_j^{II}(u_j^{II})_+ \frac{1 + \Delta t D u_j^n/2}{(1 + \Delta t D u_j^n)^2} - \frac{\Delta t}{6} D\rho_j^n \frac{(u_j^{II})^2(u_j^{II})_+}{(1 + \Delta t D u_j^n)^3}(3 + \Delta t D u_j^n), \\ F_{j-1/2}^{-(2)} &= \rho_j^{I} u_j^{I}(u_j^{I})_- \frac{1 + \Delta t D u_j^n/2}{(1 + \Delta t D u_j^n)^2} - \frac{\Delta t}{6} D\rho_j^n \frac{(u_j^{I})^2(u_j^{I})_-}{(1 + \Delta t D u_j^n)^3}(3 + \Delta t D u_j^n). \end{aligned} \tag{49}$$

For the 2D case we are dealing with, the same type of numerical method can be found in [6]. However, it is hard to find a good slope limiter which

does not still induce a large numerical diffusion. That is why we rather use a dimensional splitting of the 1D scheme previously described, with a Strang type splitting, in order to preserve the second order of the method (see [26]). In the 2D case, the scheme then takes the form :

- Transport in X direction during $\Delta t/2$
- Transport in Y direction during Δt
- Transport in X direction during $\Delta t/2$

The corresponding scheme then offers the ability to treat the delta-shocks and vacuum. Furthermore, it guaranties a maximum principle on the velocity as well as the positivity of the density. Moreover, it is second order accurate in space and in time.

4.5 Eulerian model numerical evaluation

A first step in evaluating the eulerian multi-fluid model is to evaluate its ability to capture precisely high concentration of density in the Taylor-Green vortices. Relevant information on the structure of the Eulerian droplet velocity field can then be extracted from these first simulations. Finally we analyze, in both Taylor-Green and Isotropic Homogeneous Turbulent gas flows, the behavior of the model and associated numerical method beyond the critical Stokes number and we evaluate the impact of the model in a such case.

4.5.1 Numerical efficiency and robustness of the multi-fluid

Computations in the Taylor-Green case allow us to study the ability to simulate high density concentration, and thus high mass density gradients, and to analyze the validity of our analytical Stokes criterion. We have used in our computations the uniform initial repartition in space of droplets we already introduced in the section 3.2.2. This uniform distribution with droplets equally distributed in the computational domain, is well adapted to study the robustness of the numerical method. To satisfy the mono-kinetic condition of the multi-fluid method, we have to make sure that the maximal Stokes number of the droplets remains under the critical value : $\mathrm{St}_c = 1/8\pi$ previously introduced. Otherwise, droplets would leave their initial vortices and would "cross each-other", leading to contradiction with the mono-kinetic assumption.

The point we make is related to the ability of the numerical method to capture high concentrations of droplets due to the ejection of the spray from one vortex. For the initial uniform mass density distribution, we consider a polydisperse spray and conduct the computation with the Eulerian multi-fluid model in the non-evaporating case. Since there is no evaporation, details of the droplets size

distribution, which is taken to be uniform in space, are not needed. However, we resolve the dynamics of the droplets for the whole range of sizes from zero up to the one corresponding to the critical Stokes number. The results are presented in Figure 7 for a Stokes number close to the critical one, thus exhibiting a rather complete ejection within a time one. Two successive times $t = 0.33$ and $t = 1$ in the non-dimensional setting are presented for droplets whose size correspond to 0.9 time the critical Stokes number with a spatial resolution of 100×100 cells. The numerical scheme does not encounter any difficulties even if the main part of the mass is concentrated in only a few cells.

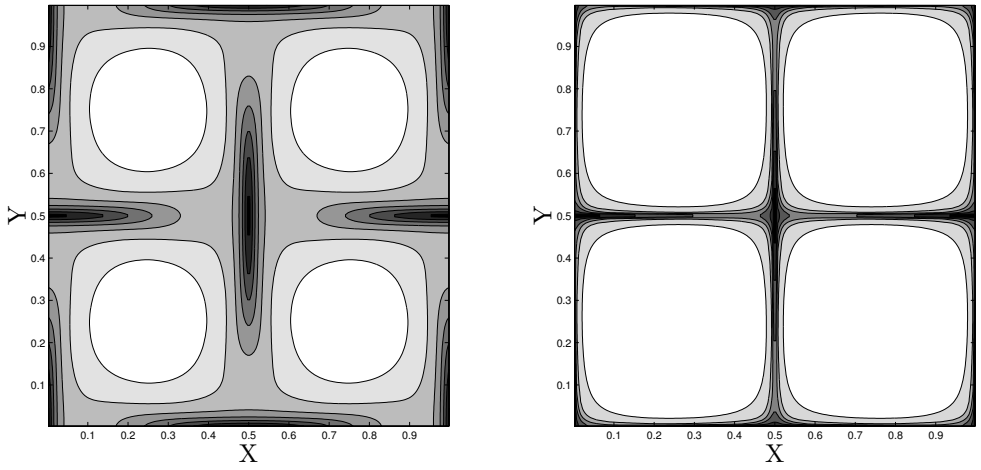

Fig. 7. Snapshots of the droplet mass density spatial distribution at times $t = 0.33$ and $t = 1.0$ during the ejection from the center of the Taylor-Green vortices to the edges for a section corresponding to $\mathrm{St} = 0.9\,\mathrm{St}_c$. The initial mass density of droplets is uniform with a zero initial velocity distribution.

To assess the order of precision of the Eulerian numerical method, we define a new initial distribution non uniform in space for the droplets. This repartition is defined thanks to the function $\psi(x) = \sin(x)/x$, for x belonging to the interval $[-\pi, \pi]$. A representation of this repartition can be done representing iso-surfaces of the number density of the droplets as in Figure 8-left.

As a matter of fact, this distribution will allow to analyze numerical diffusion of the method, and to determine the spatial refinements needed. Indeed its gradients are important as we can see in Figure 8-right where we realized a three dimensional plot to represent the droplets number density in the domain. The detailed study of the level of refinement needed to precisely reproduce the dynamics of the polydisperse spray will be conducted later on, in section 5, throughout detailed comparisons with a Lagrangian solver. This study shows the accuracy of the proposed model and numerical method within the assumptions of the multi-fluid model.

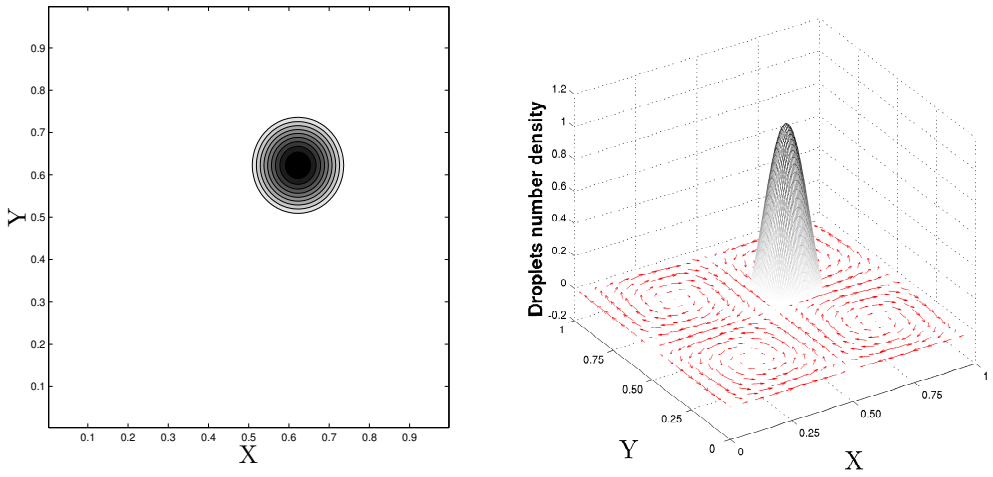

Fig. 8. Initial droplet spatial distribution : non uniform repartition in the domain, (left) number density iso-contours, (right) three-dimensional plot with number density as the third coordinate.

4.5.2 Relevant information from Eulerian simulation

Besides, as found in the previous 1D case, the droplet velocity field is rapidly attracted, within a few Stokes number, to an invariant velocity manifold, which governs the dynamics of the ejection of the spray from the vortices and is smooth only if the non-dimensional Stokes number is below its critical value. The structure of this stationary velocity field can be seen in Figure 9 in one of the Taylor Green vortex for a Stokes number beyond the critical one. In this Figure, we have presented the gaseous velocity field as well as the invariant velocity manifold for the droplets that reach the given Stokes number. One can notice that gas and droplets velocities have the same directions at the bound of the vortices. This is due to the violation of the multi-fluid mono-kinetic assumption occurring in this case. Indeed, as this computation is done with an uniform distribution of droplets with a Stokes number higher than the critical value, droplets are leaving their initial vortex and cross each-other. A mean phenomenon is thus occurring between the velocities of the droplets leaving the vortex and the droplets coming from the neighbouring vortex. It leads to droplets without any component normal to the gas velocity at the edge of the vortices as shown in details in Figure 9. Another way of considering such a manifold, keeping in mind that the main physical phenomena is the ejection of the spray from the vortex, is to plot the normal component of the droplet velocity in the frame associated with the gaseous velocity field. For example if we consider the cut presented in Figure 10-top, we can plot the normal component, that is the x-component of the droplet velocity field, for various Stokes numbers. For Stokes number close to zero, the normal velocity is globally very small, since the droplets almost follow the gaseous phase. When the Stokes number increases up to the critical value, the amplitude of the

normal component reaches a maximum while still being a continuous function of position a $x = 0$ and is responsible for the ejection of droplets and their accumulation at the edges of the vortices.

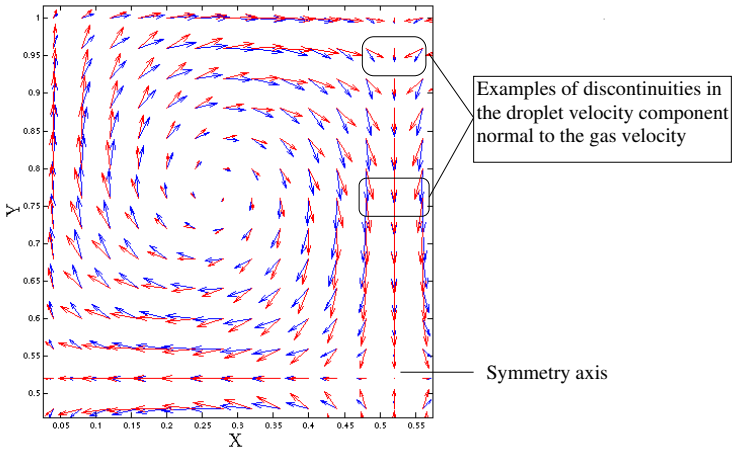

Fig. 9. (blue) Velocity vectors for a gas Taylor Green vortex, (red) velocity vectors of droplet stationary attracting velocity field for $\mathrm{St} = 4\,\mathrm{St}_c$. The fields are zoomed in the region of one vortex.

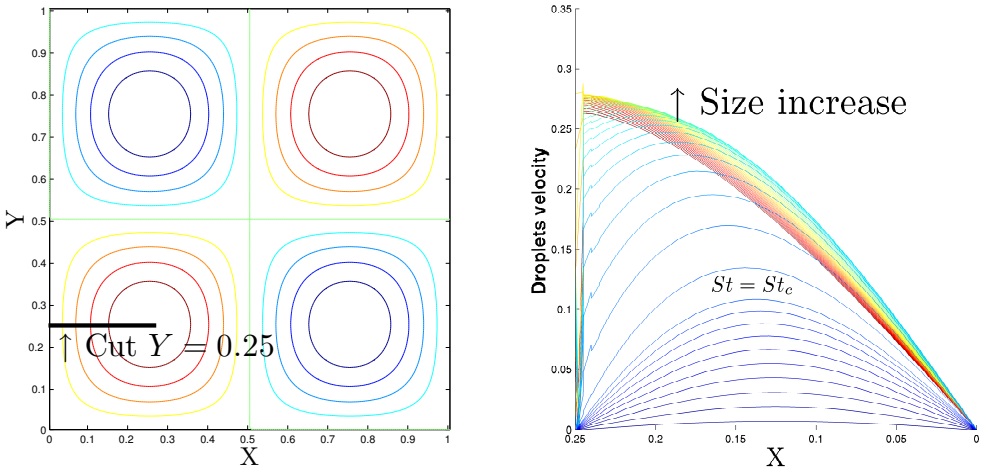

Fig. 10. (left) Stream lines of the Taylor-Green vortices and position of the cut for the study of normal ejection velocity, (right) structure of the invariant droplet velocity manifold versus Stokes number in term of the droplets velocity component orthogonal to the gas flow.

4.5.3 Numerical behavior and physical interpretation beyond the critical Stokes

Taylor-Green case If the Stokes number is increased beyond its critical value in the case of a uniform initial droplet mass density spatial distribution,

the dynamics of the spray is correctly reproduced until droplets are ejected from one vortex to the other. However, once droplets cross the lattice structure of the vortex edges, a velocity averaging phenomena, already foreseen in [24] leads, by a symmetry argument, to a zero normal mean velocity along the lattice axis. Consequently, a "δ-shock" arises at this place, that is an important concentration of droplet mass in the surrounding computational cells which are artificially trapped. After some finite time all the mass is concentrated up to numerical diffusion in the cells at the edges of the vortex lattice. Such a behavior can be clearly foreseen due to the symmetrical structure of the initial droplet mass density spatial distribution.

The non-uniform distribution (Figure 8) offers the ability to perform computations with droplets having a Stokes number greater than the critical value of $1/8\pi$ without getting into the same type of behavior (see section 3.2.2). Indeed the exit of the vortex does not lead in this case to frontal crossing of droplets originating from different vortices. This distribution will then allow us to study the behavior of more inertial droplets in a different framework.

We then performed a test case with a Stokes number $\mathrm{St} = 13\,\mathrm{St}_c$, first with a lagrangian computation. The droplets positions are presented in Figure 11, for four times. We then present in Figure 12 the dynamics of the ejection of the Eulerian mass density of the spray in the same conditions. In such a case, the spray is ejected from its original vortex, as already predicted by the analytical approach; the numerical simulation reproduces this expected behavior. Nevertheless, there is a tendency of the droplet mass distribution of such size to concentrate in very narrow regions, a phenomenon that is captured by the numerical scheme we have proposed. However, it can be seen that, during the ejection process, the artificial averaging process is already active and leads to such a high segregation of the spray. The behavior predicted by the Williams spray equation and discretized through a Lagrangian solver is slightly different as we can see in Figure 11, for time $t = 1.4$. Thus, in the framework of the Taylor-Green vortices, we have been able to produce a rather clear picture of both the numerical scheme capability and modeling limits of the transport associated with the Eulerian multi-fluid model.

Isotropic Homogeneous Turbulent case Besides, we perform computations beyond the critical Stokes in an Isotropic Homogeneous Turbulent case, in order to test the validity of this criteria in more complex gaseous flow than the Taylor-Green vortices. We consider a frozen isotropic homogeneous turbulent gas flow field. We call this "frozen" turbulence since the gaseous flow field is stationary. We represent the iso-vorticity lines of this field in Figure 13-left. To compute the critical Stokes in this configuration, we use the theory presented in section 3.2.3 and we compute the positive eigenvalue λ_+ to assess the strain rate of the flow (see Figure 13-right), and exhibit regions of high

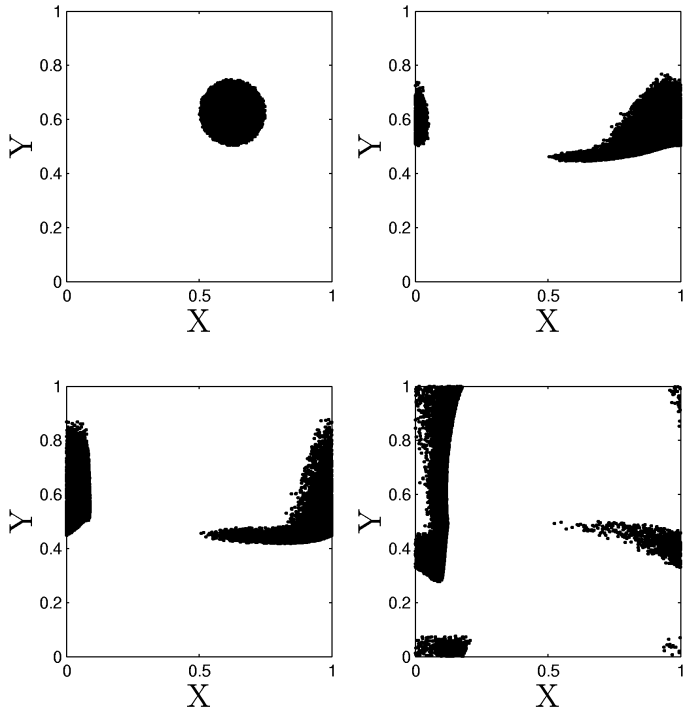

Fig. 11. Lagrangian numerical parcels position at time $t = 0$, $t = 0.8$, $t = 1$ and $t = 1.4$ in the non dimensional setting for $\mathrm{St} = 13\mathrm{St}_c$. Computation with 50000 numerical parcels.

strain rate of the flow. From this field we can compute the distribution of the eigenvalue in the flow field (PDF in Figure 14). The upper value is about 5 and the corresponding critical Stokes is then $\mathrm{St} = 1/20$.

For the sake of legibility, we focus on a small part of the domain, presented in Figure 15 for the turbulent gaseous velocity field and for the normal component of the droplet velocity with respect to the gas one. Important contra-rotating gaseous vortices are present in the considered area which are responsible for the maximal values of the strain rate in the domain (see Figure 16, similarly to the central point for the previous Taylor-Green configuration).

This part of the domain is then relevant to study droplet dynamics evolution with the Stokes number. We thus present a zoom of the gaseous vorticity field in the zone of interest as well as the gaseous velocity field in the same zone in Figures 16-left and 16-right.

Results are then presented for three Stokes numbers corresponding to 0.1 (Figure 17), 0.25 (Figure 18) and 0.5 (Figure 19). The droplet velocity field relaxes, within a non dimensional time equal to a few Stokes number, towards a velocity conditioned on the droplet Stokes number. Since we start with a zero

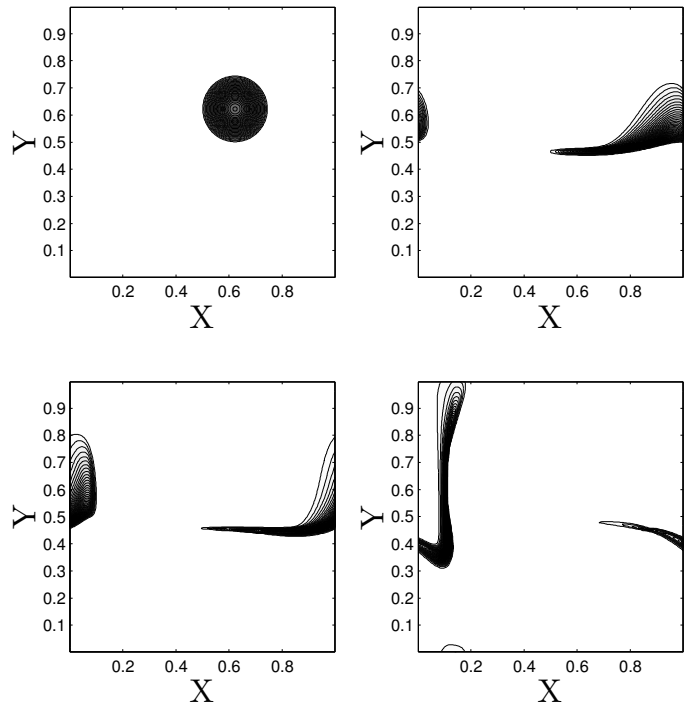

Fig. 12. Eulerian droplet mass distribution evolution at time $t = 0$, $t = 0.8$, $t = 1$ and $t = 1.4$ in the non dimensional setting for $\mathrm{St} = 13\,\mathrm{St}_c$. 55 iso-contours from 0 up to 1.66-time the maximum of the initial mass density.

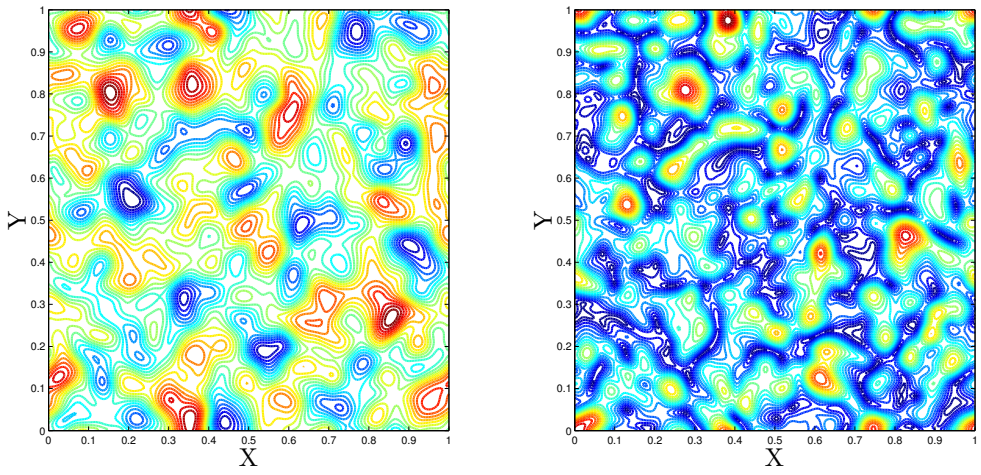

Fig. 13. (left) Frozen gaseous turbulent vorticity field; (rigth) associated strain rate λ_+. Grid 128×128.

initial velocity field, we can base our study on the invariant droplet velocity manifold at each Stokes number. Consequently, we have plotted the normal component of the droplet invariant velocity field with respect to the gaseous

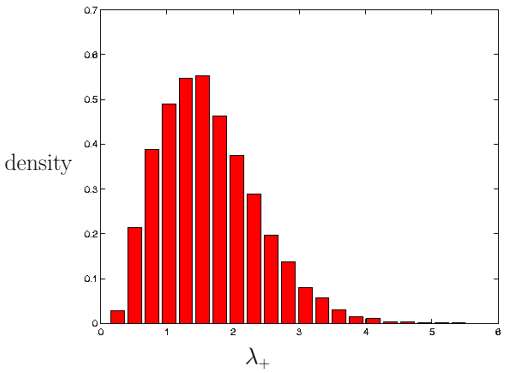

Fig. 14. Distribution of strain rate in the frozen turbulent gaseous velocity field.

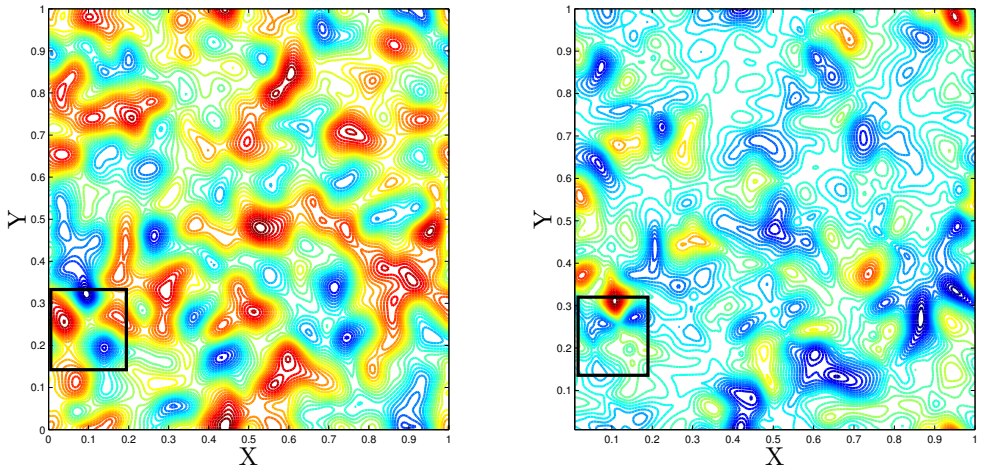

Fig. 15. (left) Frozen turbulent gaseous vorticity field, (right) Eulerian droplet velocity component orthogonal to the gas flow, for the stationary attracting field with 20 iso-contours from -0.01 to 0.015 , at time $t = 3$ in the non dimensional setting and for $\mathrm{St} = 0.1$.

velocity field on the left. On the right of each Figure for the three Stokes numbers, we present the two vector fields, for both the droplets and the gas, with a zoom in the zone of highest strain rate.

When we start with a Stokes number which is 0.1, that is twice the obtained critical Stokes, the amplitude of the normal component of the droplet velocity field with respect with the gaseous field can be shown to be small (see Figure 17 left and right). However, when the Stokes number is close to the critical value, the ejection process from the vortices and the resulting discontinuity is rather weak; such a statement can be shown precisely in the 1D and Taylor-Green vortices cases. Even if there is an impact of this discontinuity on the number density field dynamics, this impact will be very limited.

When the Stokes number reaches 0.25, it is clear from the graphs in Figure 18

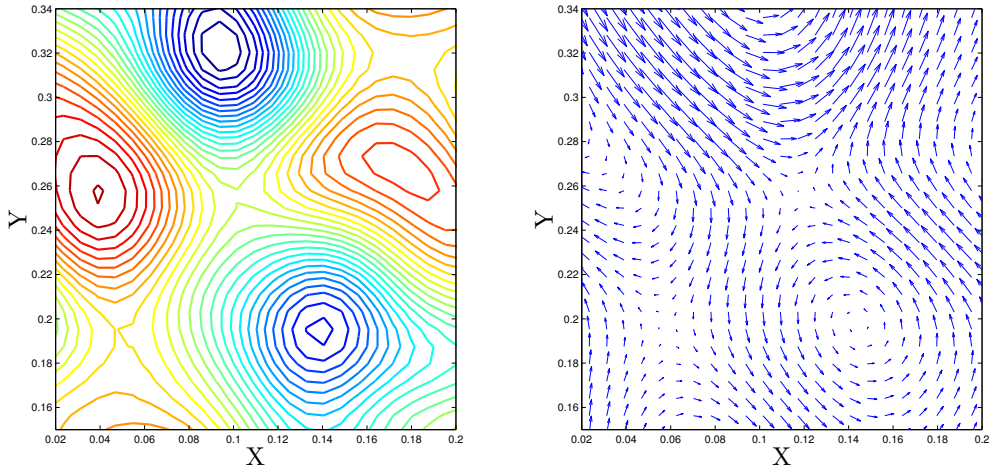

Fig. 16. (left) Frozen turbulent gaseous vorticity field, (right) frozen turbulent gaseous velocity field, at time $t = 3$ in the non dimensional setting. The fields are zoomed in the area of interest

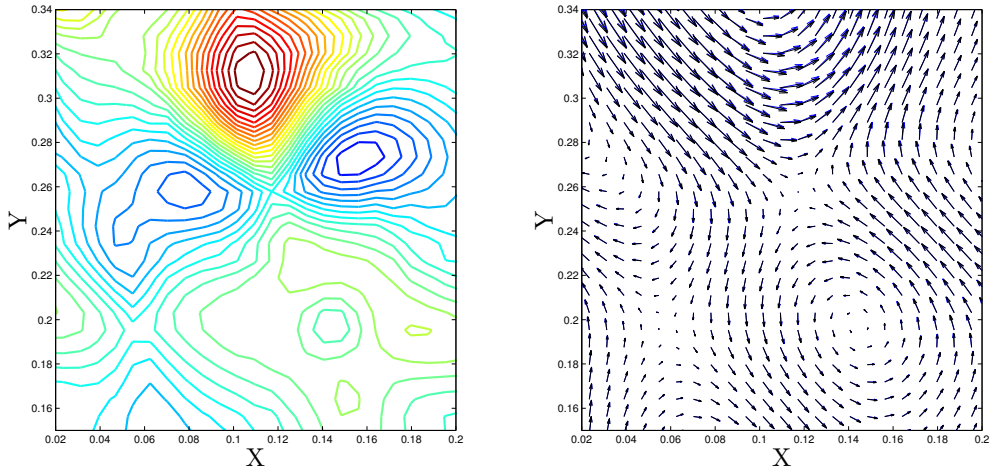

Fig. 17. (left) Eulerian droplet velocity component orthogonal to the gas flow for the stationary attracting field, at time $t = 3$ in the non dimensional setting for St = 0.1. 20 iso-contours from -0.011 up to 0.017; (right) vector representation of both droplet (black) and gas (blue) velocities for the same time. Both fields are zoomed in the area of interest.

that a singularity in the droplet velocity field appears; the range of values of the normal velocity starts growing and, at the scale of the spatial resolution provided for this example in the neighborhood of the highest strain rate point, a discontinuity arises. This velocity discontinuity leads to crossing droplets. Such a behavior will become even stronger for a Stokes number of 0.5, that is ten times the critical value, for which a strong discontinuity has formed in Figure 19-left for the normal component of the droplet velocity field. Even in Figure 19-right, one can observe some arrows having opposite directions in the

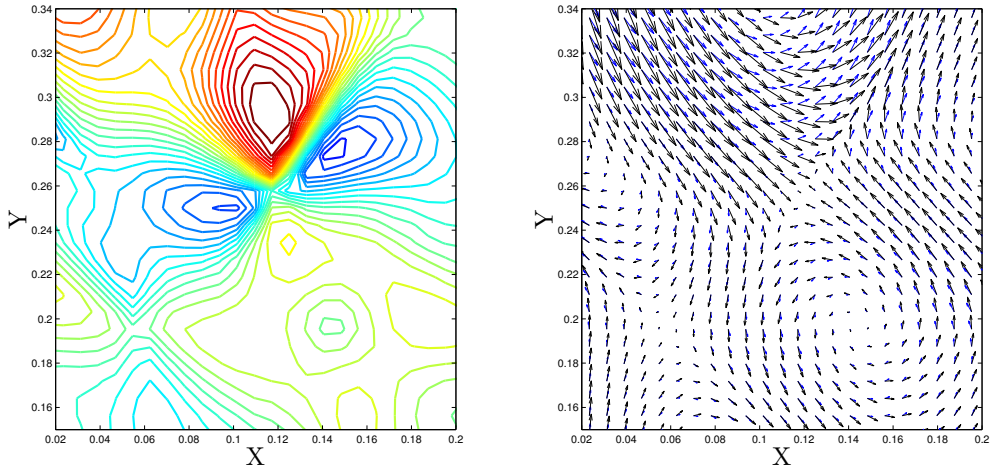

Fig. 18. (left) Eulerian droplet velocity component orthogonal to the gas flow for the stationary attracting field, at time $t = 3$ in the non dimensional setting for $\mathrm{St} = 0.25$. 20 iso-contours from -0.08 up to 0.1; (right) vector representation of both droplet (black) and gas (blue) velocities for the same time. Both fields are zoomed in the area of interest.

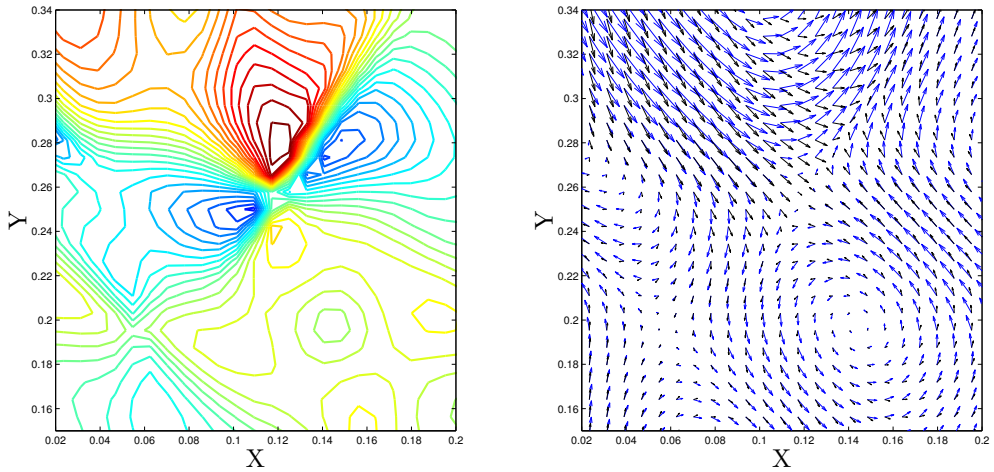

Fig. 19. (left) Eulerian droplet velocity component orthogonal to the gas flow for the stationary attracting field, at time $t = 3$ in the non dimensional setting for $\mathrm{St} = 0.5$. 20 iso-contours from -0.14 up to 0.16; (right) vector representation of both droplet (black) and gas (blue) velocities for the same time. Both fields are zoomed in the area of interest.

neighborhood of the highest strain rate point.

We can then conclude that the observed behavior is still the same in this more complex configuration and leads to the same conclusions as before. First the numerical method is able to cope with such difficulties and can capture the singularities appearing in the Eulerian model without leading to unstable

solutions. We have to keep in mind that in the case of dilute sprays, the creation of such singularities relates to a failure of the modeling to reproduce the physical behavior of the spray. However, it seems reasonable to think that the limitation of the multi-fluid model associated with the mono-kinetic character of the droplet velocity field will only be of real importance when strong discontinuities appear, that is much above the critical Stokes number. In a such case, we will need extra modeling at the Eulerian level as well as at the kinetic level where eventual interactions between droplets have to be considered depending on the levels of droplet number density.

5 Lagrangian versus Eulerian spray simulations : accuracy and computational cost

This section is divided into two parts. The first one is devoted to a detailed comparative study of the accuracy of the two methods with one-way coupling and various gaseous flow fields. We restrict ourselves to one-way coupling for comparisons purposes. Such a comparison will mainly be conducted on the Taylor-Green configuration, since it is a representative test case, for both a non evaporating and an evaporating case. The two approaches are quite heterogeneous. This implies a precise definition of what should be compared in order to draw firm conclusions from the study. Second, once we understand, for a given level of accuracy, what should be the level of discretization for both approaches, we can conduct a relevant comparison of the associated computational cost. This is first done in the context of the Taylor-Green vortices, but it is, at that level, important to conduct such a study on the turbulent configuration since the interpolation of the gas properties along the particle trajectories have a strong impact on the computational cost of the Lagrangian methods.

5.1 Comparison of the accuracy

We present first precise and quantitative comparisons between the Lagrangian and the Eulerian descriptions for the Taylor-Green vortices where the analytical gaseous velocity field as well as the polydisperse spray initial condition provide a challenging test case and are representative of the main problems we will encounter in more complex configurations. The first ingredient is to define a procedure to be able to compare the accuracy of both methods; we then use it for both a non-evaporating and an evaporating case. We will then present the results we obtained concerning comparisons in an Isotropic Homogeneous Turbulence configuration.

5.1.1 Comparison procedure

To evaluate differences between the two spray solutions, given a gaseous velocity field, we need to reconstruct Eulerian fields from the statistical information provided by the Lagrangian treatment. We thus need to define an Eulerian grid to perform this reconstruction. Furthermore, as we want to compare the Lagrangian results to the Multi-Fluid ones, we want to perform comparisons for various droplet sizes to study the ability of the Eulerian method to capture dynamics of droplets of various sizes. In our two dimensional Taylor-Green case, we need a three-dimensional grid to account for space and size discretizations. We have chosen in this case a $100 \times 100 \times 10$ grid, to have a sufficiently detailed description of the fields : 100×100 for the space discretization, and 10 size intervals to be able to study polydispersity. Computing errors on this grid means :

- rebuilding the Eulerian fields for the mass densities in the size intervals from the Lagrangian statistics on this grid;
- averaging, if necessary, the Eulerian Multi-Fluid results on this very grid.

An example of such a reconstruction is to be found in Figure 20 where a zoom is presented (we have focused on a quarter of the computational domain, which is the zone of interest).

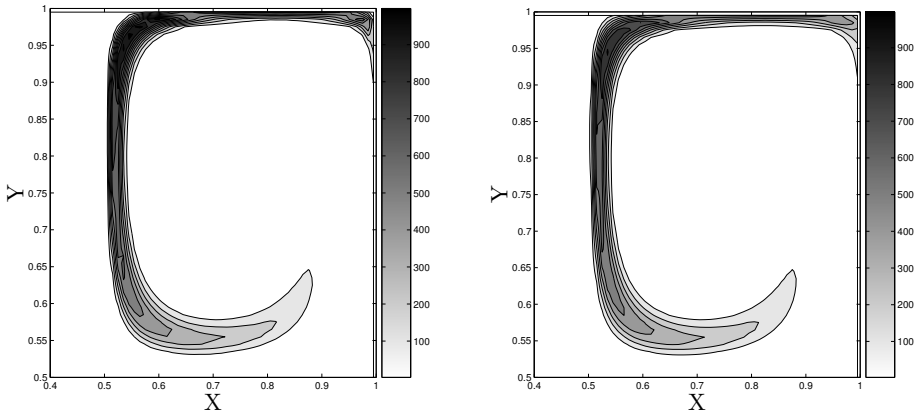

Fig. 20. Zoom on a quarter of the periodic computational domain of the total mass density of droplets at time $t = 1.5$, projected on the comparison grid $100 \times 100 \times 10$: (left) Lagrangian reference solution (right) Eulerian with a $400 \times 400 \times 10$ grid.

We evaluate on this grid the global error at the time $t = 1.5$ (i.e. $t = 1.5\,\tau_{gas}$, about one and a half eddy turn over time). The constant by pieces error field for a generic quantity Q, which in the following will be mainly the droplet mass density in one section, is defined for an Eulerian computation by:

$$E_Q^{1.5}(x, y) = Q_{\mathrm{e}}^{1.5} - Q_{\mathrm{l-ref}}^{1.5}, \tag{50}$$

where the fields are taken to be constant inside a cell of the comparison grid. The right-hand-side corresponds to the averages over the associated cell of both the Eulerian simulation (subscript e) and the Lagrangian reference simulation with 16 Million particles (subscript $\mathrm{l}-\mathrm{ref}$), respectively.

To have an estimate of the relative error over the whole grid, we study the L^1 norm of the relative error on the grid :

$$||E_Q^{1.5}||_1 = \frac{\int_0^1 \int_0^1 |Q_{\mathrm{e}}^{1.5}(x,y) - Q_{\mathrm{l-ref}}^{1.5}(x,y)|\mathrm{d}x\mathrm{d}y}{\int_0^1 \int_0^1 |Q_{\mathrm{l-ref}}^{0}(x,y)|\mathrm{d}x\,\mathrm{d}y}. \tag{51}$$

The denominator is taken at the initial time, but this has no impact on the non-evaporating case since the global mass as well as the mass in the sections are preserved throughout the calculation. For the evaporating case, this has however an impact and allows to quantify the error relative to the initial amount of mass, which is the one with the main physical sense.

5.1.2 Non Evaporating spray

To illustrate comparisons between the Eulerian and the Lagrangian methods previously described, we present a study of the error between the Lagrangian reference case with 16 Million particles and the Eulerian cases, to show that both methods converge towards the same results. The chosen time for the comparison is $t = 1.5$, for which the total mass density is presented in Figure 20. It exhibits a high concentration of the inertial droplets around the vortex and creates very high gradients. It is thus a really challenging test case as far as Eulerian models are concerned, irrespective of the evaporation process. We now discuss the error plots presented in Figures 21 to 23 where the details of the comparisons are conducted for three representative sections illustrating the influence of the droplets inertia on their behavior. The pictures represent the evolution of the logarithm of the relative error between Eulerian multi-fluid cases and the reference Lagrangian computation versus the logarithm of the space discretization step of the Eulerian computation. For convenience, we have presented the actual values of the error and of the space discretization step on the two axis, but the points on these axis correspond to the logarithms of these values. As we mentioned in Section 2, the numerical method used for the multi-fluid model is second order in space, explaining the line with a slope equal to two in all the pictures. The plots show three different levels of space refinements for the Eulerian computation : 100×100, 200×200 and 400×400. In order to see the influence of the refinement in size of the Multi-Fluid model, we plot three curves in each Figure, showing three size discretizations : 10 sections, 20 sections and 30 sections.

Concerning the droplets of intermediate size presented in Figure 22, the Eulerian computation converges towards the Lagrangian reference case with almost

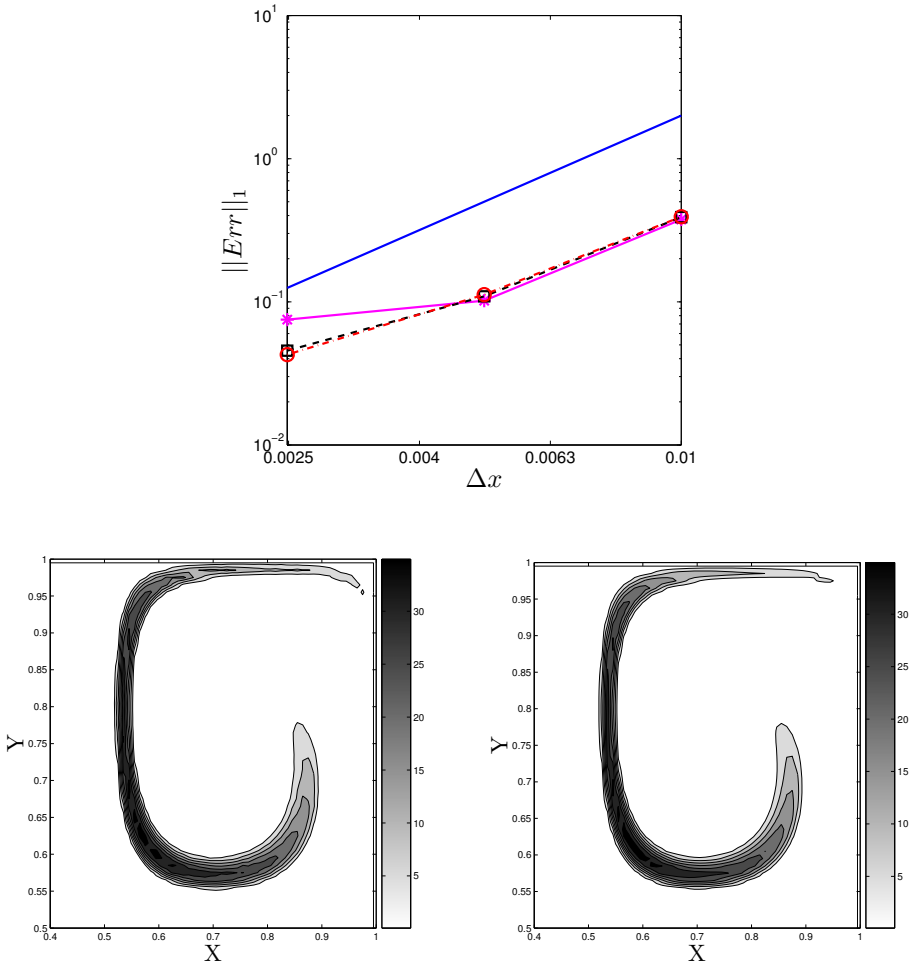

Fig. 21. (top) Logarithm of L^1 norm of the error between Eulerian simulation for small droplets (second section $\mathrm{St} = 0.14\,\mathrm{St}_c$) for various Δx and the Lagrangian reference solution at time $t = 1.5$, projected on the comparison grid $100 \times 100 \times 10$: slope two line (blue solid line), 10 sections (solid line), 20 sections (dashed line) and 30 sections (dotted-dashed line). (bottom) Corresponding droplet mass density with 10 iso-contours from 0 up to 1.44-time the maximum of the initial mass density in the second section : (left) Lagrangian reference solution, (right) Eulerian computation with a $400 \times 400 \times 10$ grid.

second order. Furthermore, ten sections are enough for the size discretization since the size refinement does not have any impact on the global error. The effect of the size discretization step refinement in this non-evaporating case is purely a finer description of the velocity distribution as a function of droplet size for a given location and time. Consequently, in the range of Stokes number associated to these droplets of intermediate size, the size-dependence of the velocity field is not strong enough to require a finer discretization and the dynamics of the droplets are correctly reproduced by the 10 sections case.

For more inertial droplets, Figure 23, the order of convergence is weaker and

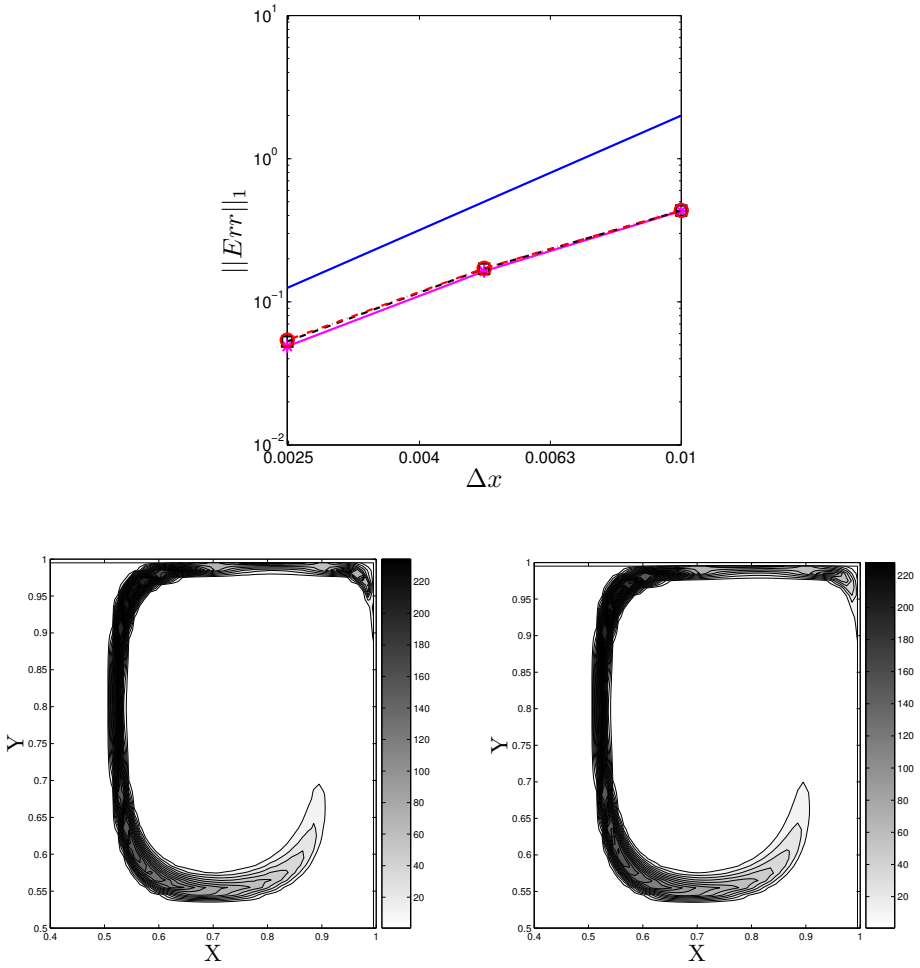

Fig. 22. (top) Logarithm of L^1 norm of the error between Eulerian simulation for medium size droplets (fifth section $\mathrm{St} = 0.41\,\mathrm{St}_c$) for various Δx and the Lagrangian reference solution at time $t = 1.5$, projected on the comparison grid $100 \times 100 \times 10$: slope two line (blue solid line), 10 sections (solid line), 20 sections (dashed line) and 30 sections (dotted-dashed line). (bottom) Corresponding droplet mass density with 10 iso-contours from 0 up to 1.44-time the maximum of the initial mass density in the fifth section : (left) Lagrangian reference solution, (right) Eulerian computation with a $400 \times 400 \times 10$ grid.

it is not improved by the refinement in section. As a matter of fact, this is due to the high gradient appearing for this class of droplets; indeed the inertial droplets are quickly ejected from the vortex and form high concentration regions and therefore very high gradients (most of the mass is concentrated in a few cells). In this case, the numerical method reduces its order of precision to first order to deal with such concentrations and associated gradients, thanks to the use of a slope limiter we presented in section 4.4. When we increase the number of points we decrease these gradients and we therefore increase the order of the method, as represented in the Figure 23.

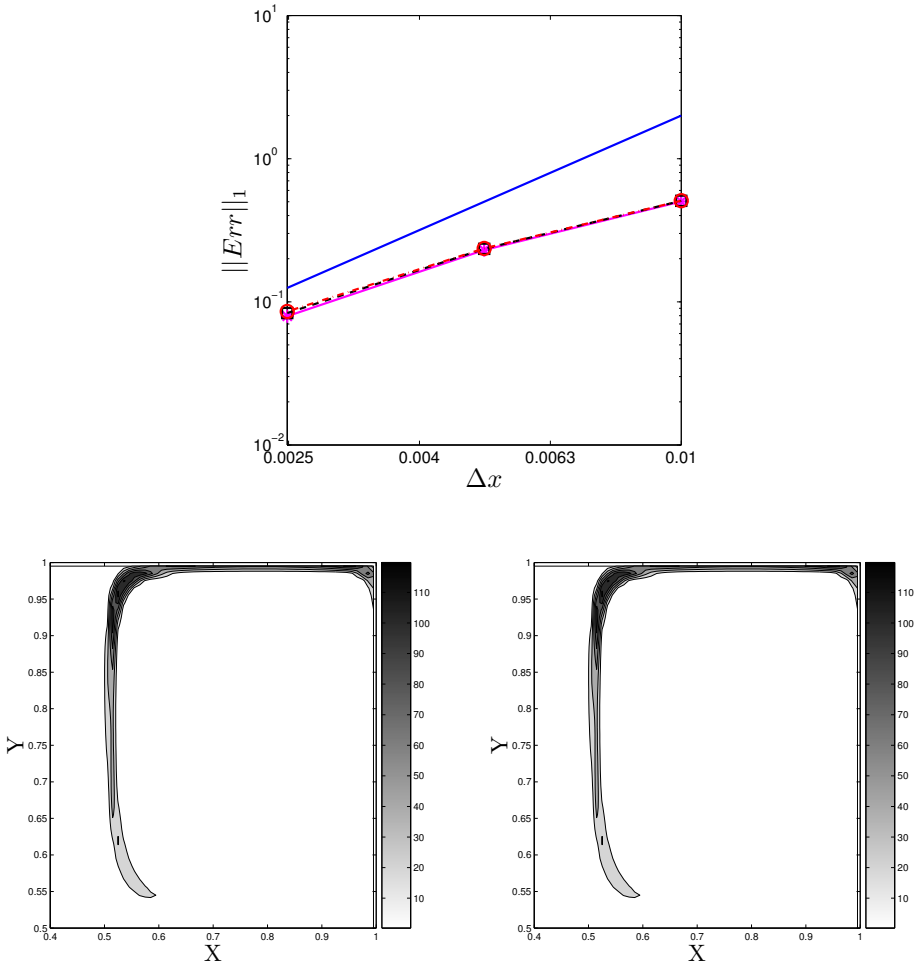

Fig. 23. (top) Logarithm of L^1 norm of the error between Eulerian simulation for medium size droplets (ninth section $\mathrm{St} = 0.78\,\mathrm{St}_c$) for various Δx and the Lagrangian reference solution at time $t = 1.5$, projected on the comparison grid $100 \times 100 \times 10$: slope two line (blue solid line), 10 sections (solid line), 20 sections (dashed line) and 30 sections (dotted-dashed line). (bottom) Corresponding droplet mass density with 10 iso-contours from 0 up to 2.43-time the maximum of the initial mass density in the ninth section : (left) Lagrangian reference solution, (right) Eulerian computation with a $400 \times 400 \times 10$ grid.

As far as the small droplets are concerned, Figure 21, the behavior is different from the previous ones. Indeed we notice an important influence of the droplet size refinement in the rate of convergence. In this case with droplets of low inertia, the build up of the overall droplet mass density spatial gradients does not build up to strongly so that the change in order is not due to excessive gradients created by the droplet rapid ejection from the vortices; nevertheless the droplet velocity is close to the gas one, but the velocity difference between spray and gas can be shown to be linear, in first approximation, with respect to the Stokes number and, thus one can guess (see figure 10) that the velocity conditioned by droplet size is a linear function of droplet surface around zero.

The assumption of the multi-fluid (see section 2) imposes a velocity which is constant as a function of size inside a section and thus it is not able to capture this effect. Then we have to switch to 20 sections to properly predict the dynamics of droplets with very low inertia. Once refined in size, the Eulerian computation converges towards the Lagrangian reference with an order of about 2.

Both descriptions are thus presenting a very good agreement as we can see quantitatively by analyzing the error levels. The L^1 norm of the error is around a few percent for a Eulerian simulation with a $400 \times 400 \times 10$ discretization as summarized in Table 1. Such an error can be thought of as rather high. It can be explained in the following way. We have chosen to present the relative error in reference of the initial total mass introduced in the numerical simulation, we have a small amount of mass concentrated in a narrow region of the domain which gets even more concentrated due to the ejection process by the vortex and finally, we have extreme gradients in order to test the influence of the numerical diffusion of the second order in space numerical method. If, however we decided to plot the absolute error only considering that the mass density of droplets is reaching one at its maximum, we would end up with an error of about one per a thousand. Such a statement can be observed more qualitatively, plotting the iso-contours of the mass density for the three sections studied in Figures 21, 22 and 23. Dynamics of the droplet of various sizes are very well predicted, even if the chosen test case is extremely challenging and leads to the presented level of errors.

Droplet size	Global error norm $\|\|E_m^{1.5}\|\|_1$
$\mathrm{St} = 0.14\,\mathrm{St}_c$	8%
$\mathrm{St} = 0.41\,\mathrm{St}_c$	5%
$\mathrm{St} = 0.78\,\mathrm{St}_c$	8%

Table 1
Computation of $||E_m^{1.5}||_1$, norm of the global error at time $t = 1.5$, for the mass density of three sections of droplets in size : small droplets ($\mathrm{St} = 0.14\,\mathrm{St}_c$), medium size droplets ($\mathrm{St} = 0.41\,\mathrm{St}_c$) and inertial droplets ($\mathrm{St} = 0.78\,\mathrm{St}_c$).

5.1.3 Evaporating case

Our interest being in combustion applications, we perform similar comparisons in the evaporating case, the evaporation being described by a d^2 law in both Eulerian and Lagrangian descriptions (see section 2). We still refer to a Lagrangian computation with 16 Million particles. To do so, we have chosen a low evaporation speed to preserve a relatively high number of particles in our reference computation. We then chose an evaporation constant $\mathrm{E_v} = 1/15$ (introduced in section 2), thus if we look at non dimensional $t = 1.5$, 10% of

the mass will be evaporated. We present in this case the errors already defined for the non evaporating case between Lagrangian and Eulerian descriptions. We study the same mesh refinements for the Eulerian method, in space as well as in size, and we study the behavior of various droplet sizes.

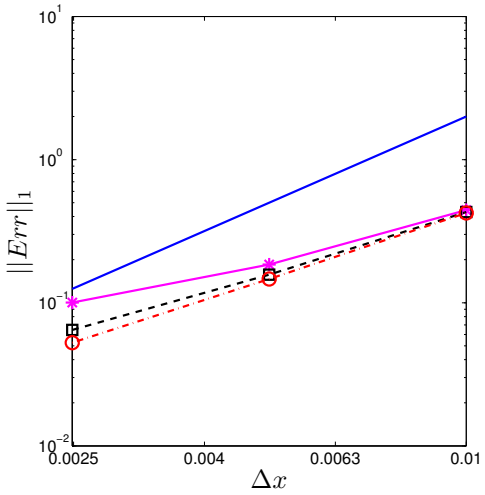

Fig. 24. Logarithm of L^1 norm of the error between Eulerian simulation for small droplets (second section $\mathrm{St} = 0.14\,\mathrm{St}_c$) for various Δx and the Lagrangian reference solution at time $t = 1.5$, projected on the comparison grid $100 \times 100 \times 10$ in the evaporating case : slope two line (blue solid line), 10 sections (solid line), 20 sections (dashed line) and 30 sections (dotted-dashed line).

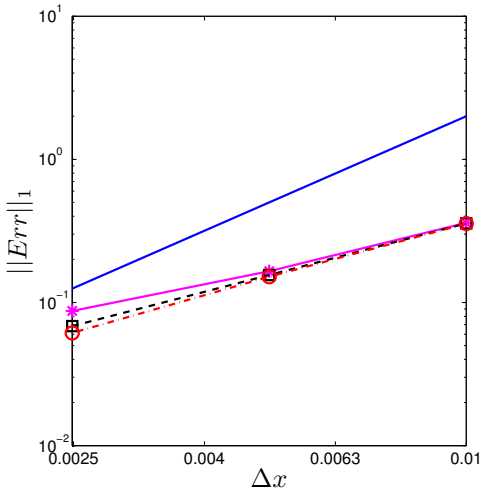

Fig. 25. Logarithm of L^1 norm of the error between Eulerian simulation for medium size droplets (fifth section $\mathrm{St} = 0.41\,\mathrm{St}_c$) for various Δx and the Lagrangian reference solution at time $t = 1.5$, projected on the comparison grid $100 \times 100 \times 10$ in the evaporating case : slope two line (blue solid line), 10 sections (solid line), 20 sections (dashed line) and 30 sections (dotted-dashed line).

We see in the Figures 24 and 25 that the behavior of small and intermediate droplets is the same as in the non evaporating case : the Eulerian method converges towards the Lagrangian reference solution with the expected second order. On the other hand, for the inertial droplets, the refinement in space nearly do not change the error value, only modified by the refinement in sizes, as we can see in Table 2.

$1/\Delta x$	Error 10 Sections	Error 20 Sections	Error 30 Sections
100	25%	14%	10.5%
200	25%	15%	11%
400	25%	15%	11%

Table 2
Evolution of L^1 norm of the relative error between the reference Lagrangian solution and Eulerian multi-fluid for various refinements in space and size, projected on the comparison grid $100 \times 100 \times 10$, and for inertial droplets ($\mathrm{St} = 0.78\,\mathrm{St}_c$). The results are presented at time $t = 1.5$

As we introduced in section 2, the multi-fluid model for evaporation is only first order accurate in the size discretization step [23]. This explain why we do not see the effect of the space refinement, hidden by the need to increase the number of cells/sections in the size phase space. This first order of the evaporation model can be illustrated by the same type of log/log Figure as we presented so far, but taking the logarithm of the size refinement, at fixed space disretization varying between $\Delta x = 1/100$ and $\Delta x = 1/400$. This is done in Figure 26.

This drawback of the multi-fluid method was already noticed in [25] and can be partially avoided by using a second order method to describe the evaporation as described in [23] and [13]. These techniques are not presented in this paper because new methods based on a breakthrough from classical multi-fluid are in the process of being developed [28] and yield a very efficient description of the evaporation process. As a conclusion, we have shown in both the evaporating and non-evaporating cases the ability of the multi-fluid model to accurately approximate the Lagrangian reference solution, and thus the dynamics of droplets of various sizes coupled to the evaporation process. Even if some improvement of the description of the evaporation process is to come, we can still define an equivalent level of accuracy for both descriptions and thus come up with a relevant information as far as computational cost is concerned.

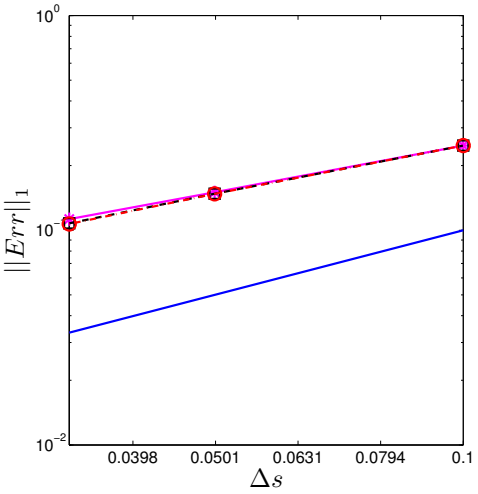

Fig. 26. Logarithm of L^1 norm of the error between Eulerian simulation for inertial droplets (ninth section $\mathrm{St} = 0.78\,\mathrm{St}_c$) for various ΔS at fixed Δx and the Lagrangian reference solution at time $t = 1.5$ projected on the comparison grid $100 \times 100 \times 10$ in the evaporating case : slope one line (blue solid line), $\Delta x = 1/100$ (solid line), $\Delta x = 1/200$ (dashed line) and $\Delta x = 1/400$ (dotted-dashed line).

5.1.4 Turbulent case

The Taylor-Green configuration can be considered to be a challenging test in the sense that it involves very high gradients of the number density function. Thus the results obtained in the previous part of this section can be considered as reliable in terms of accuracy of the methods. However, to show the ability of the Eulerian model to capture turbulent configurations, we also provide some more qualitative comparisons in the case of a frozen Isotropic Homogeneous Turbulence. This second configuration will prove to be useful in terms of computational cost comparisons. The vorticity of the selected gas field is represented in Figure 27-left.

We performed Lagrangian and Eulerian computations with a polydisperse spray and an initial uniformly distributed NDF as far as space is concerned (as described in section 3.2.2). We present in Figure 28 the Eulerian and Lagrangian total mass distribution at the non dimensional time $t = 1.5$. Computations are done with 4 Million particles for the Lagrangian and a $256 \times 256 \times 10$ grid for the Eulerian. We represent, in this figure, the total mass distribution, i.e sum over all the size intervals.

These first results show a very good qualitative agreement between the Lagrangian and Eulerian descriptions. We can observe the segregation effect of the vortices on the spray mass density distribution, the structure of which corresponds clearly to the iso-vorticity lines of the gaseous phase. The ejection of the droplet mass density from the vortical structures generates region of high

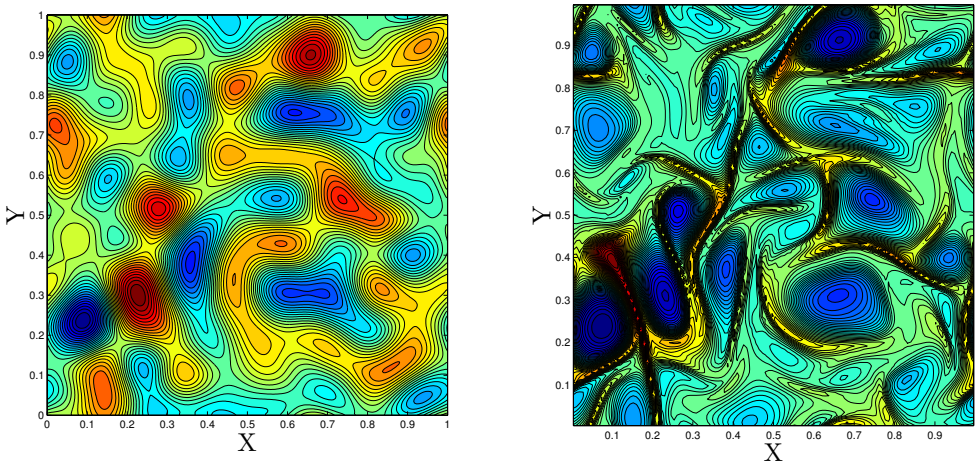

Fig. 27. (left) Frozen turbulent gaseous vorticity field; (right) Eulerian total mass density of the spray at time $t = 1.5$ with 50 iso-contours between 0 and 25-times the initial uniform level.

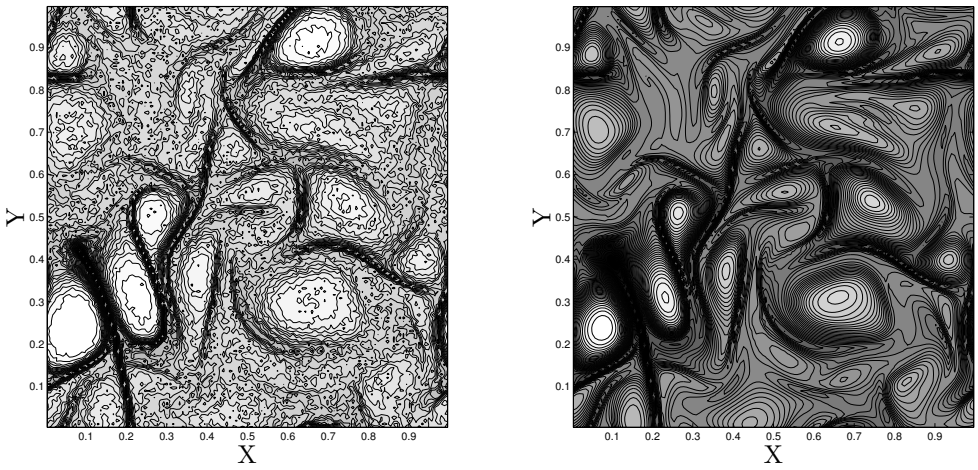

Fig. 28. Total mass density spatial distribution at $t = 1.5$, projected on a $128 \times 128 \times 10$ comparison grid with 50 iso-contours between 0 and 25-times the initial uniform level which is the same for both computations: (left) Eulerian with a $256 \times 256 \times 10$ grid; (right) Lagrangian with 4 Million particles.

density and creates very large density gradients, which are both described precisely by the two methods. This is not the purpose to reproduce the same kind of analysis as before for this second case. It is shown for illustration purposes in terms of precision since it is not as challenging as the Taylor-Green configuration, however it will prove a very useful test case in terms of computational evaluation of the two methods in the next section.

5.2 Computational efficiency

In fact, the question of the computational efficiency has to cover many topics. The first key question is the cost of both Lagrangian and Eulerian models of unsteady configurations (a common question for one-way or two-way coupling) as well as the choice of numerical methods and algorithms to perform such a comparison. This issue is at the heart of the present paper; with the information brought in the previous part, we can now tackle the question of the computational cost comparison within the framework of the Taylor-Green configuration in a first paragraph. However, a second issue is the cost of the coupling of the two phases and the associated numerical methods. It also involves two subquestions; the first one is based on the exchange of information from the gas to the disperse liquid phase in order to predict its dynamics in the phase space and an interesting study is conducted in a second paragraph within the framework of the frozen turbulent flow. The final question is related to the two-way coupling of the phases and its impact on the global computational cost. We come to this issue in the last paragraph.

5.2.1 Taylor Green case

One should notice that the Taylor-Green configuration studied so far, though very adequate to perform the quantitative comparisons we presented in the previous section, only partially allows a comprehensive study of the computational cost. However we will compare the costs associated to the different descriptions in this configuration and then discuss the results before switching to a more representative configuration.

We take the Lagrangian computation with 16 Million particles as a reference and we find, as summarized in Table 3 that we have a comparable precision to that reference with a Lagrangian computation with 2 Million particles and with an Eulerian Multi-Fluid computation on a $400 \times 400 \times 10$ grid. The computational costs of these two computations are rather the same (see Table 3), the Eulerian being almost 10% faster. The computation costs given in Table 3 are obtained on a slot of a AMD64 opteron dual core 275 (2.19GHz) with a 8Go memory. Nevertheless these first results have to be analyzed before concluding. First of all we have to recall that the configuration we study is, for modeling purpose, a simple one compared to a more realistic configuration. Consequently the refinement we used, for both the Lagrangian and the Eulerian computations, would be far too expensive for a realistic application. Indeed we are describing a single gas vortical structure with 2 Million particles in the Lagrangian case and 200×200 points, (a quarter of 400×400) in the Eulerian case. These refinements have been used for the study of the convergence of both methods but they could no longer be used in a realistic case.

	Error $0.14\,\mathrm{St}_c$	Error $0.41\,\mathrm{St}_c$	Error $0.78\,\mathrm{St}_c$	CPU Time(s)
Lagrangian	7.8%	4.5%	5.5%	5470
Eulerian	7%	5%	12%	4670

Table 3
L^1 norm of the relative error between Lagrangian with 2 Million particles and Eulerian Multi-Fluid on a $400 \times 400 \times 10$ grid, both compared to the Lagrangian 16 Million particles reference on the comparison grid $100 \times 100 \times 10$. Three sections are studied : small droplets ($\mathrm{St} = 0.14\,\mathrm{St}_c$), intermediate droplets ($\mathrm{St} = 0.41\,\mathrm{St}_c$) and inertial droplets ($\mathrm{St} = 0.78\,\mathrm{St}_c$). The results are presented at time $t = 1.5$.

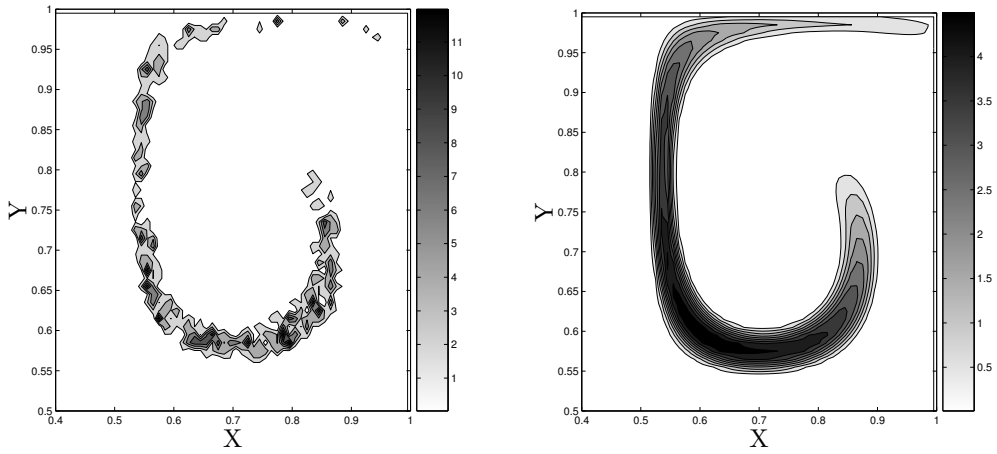

Fig. 29. Mass density of droplets of small size (second section $\mathrm{St} = 0.14\,\mathrm{St}_c$) at time t=1.5, projected on the comparison grid $100 \times 100 \times 10$: (left) coarse Lagrangian simulation with 10^5 particles; (right) coarse Eulerian simulation with a $100 \times 100 \times 10$ grid.

We can then reduce the level of refinement and take for example a refinement around 16 times coarser : a Lagrangian simulation with 100000 particles and an Eulerian Multi-Fluid computation with a $100 \times 100 \times 10$ grid, to see the behavior of the methods with a coarser discretization.

We notice the outbreak of oscillations in the Lagrangian computations, for the extreme sizes of the distribution as well as for the intermediate sizes. Small droplet case is showed in Figure 29 through an iso-contour of mass, and inertial droplets in Figure 30 through a three dimensional plot with the mass level as the third dimension of the graph. These oscillations could bring in difficulties in term of the phase coupling for combustion applications, for example when trying to describe as precisely as possible the fuel mass fraction in the gaseous phase issued from the evaporation process. On the other side, the coarse Eulerian computation induces more numerical diffusion, less prejudicial than the

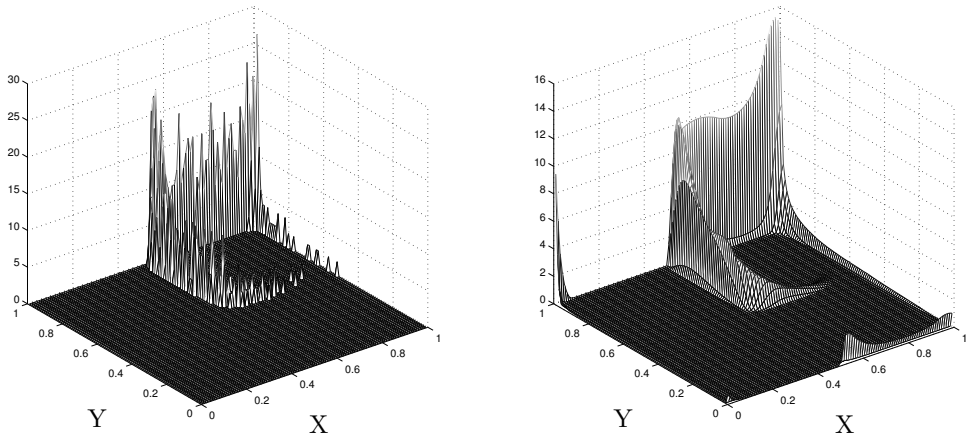

Fig. 30. Mass density 3D plots of inertial droplets (ninth section $\mathrm{St} = 0.78\,\mathrm{St}_c$) at time t=1.5, projected on the comparison grid $100\times100\times10$: (left) coarse Lagrangian simulation with 10^5 particles; (right) coarse Eulerian simulation with a $100\times100\times10$ grid.

Lagrangian oscillations, but still observed in Figure 30.

Nevertheless, even if a finer discretization is used, the comparison we have conducted is in fact restricted to one part of the computational cost, that is the one purely related to the transport in phase space of the spray, once the coupling terms with the gaseous phase are known (drag, evaporation,...). However, another source of computational cost is to be found in the interpolation of the gaseous velocity, mass fraction, temperature fields either along the droplet trajectories, or at the Eulerian cells. In this context, we switch to the frozen turbulent case.

5.2.2 Turbulent case

Indeed, as we already said, the gaseous phase is analytically known for the Taylor-Green configuration so that in the Lagrangian computation, there is no need to interpolate in order to compute the velocity of the gas at the drop location. In the frozen turbulent case, however, the gaseous field comes from a numerical simulation and only discrete values are known thus interpolation is necessary. Consequently, we have decided to realize an evaluation of the computational costs of both description in the case of Homogeneous Isotropic Turbulence. The first cost evaluation we made is presented in Tables 4 for the Lagrangian method and 5 for the Eulerian one. Therefore for a refined Eulerian computation (grid $512^2 \times 10$) the cost is six times lower to the Lagrangian computation with 4 Million particles, that still presents some oscillations as seen in Figure 28. Nevertheless, one has to notice that if the gas phase is solved on a coarser grid than the Eulerian multi-fluid computation, it will be

Lagrangian refinement	1 Million parcels	2 Million parcels	4 Million parcels
CPU cost (s)	$1.68e4$	$3.21e4$	$6.40e4$

Table 4
Computational cost for the frozen Isotropic Homogeneous Turbulence case for the Lagrangian method as a function of the number of numerical parcels introduced and for $t \in [0, 3]$.

Space refinement Size refinement	256×256	512×512
10 sections	$6e2$	$5.0e3$
20 sections	$1.3e3$	$1.00e4$

Table 5
Computational cost for the frozen Isotropic Homogeneous Turbulence case for the Eulerian multi-fluid method as a function of the grid refinement in space and time and for $t \in [0, 3]$.

necessary to interpolate the gas velocity. Yet, as the grid do not evolve during the computation, the cost of this operation is not going to be prohibitive.

Furthermore we can notice that the structure of the Eulerian multi-fluid model will allow us to parallelize efficiently the computation, for example distributing the transport resolution of the various sections to multiple processors. This will increase very significantly the efficiency of the Eulerian computation and authorize to refine consistently still having a low cost compared to the Lagrangian solver.

5.2.3 Two-way coupling and further investigations

In the present paper, since we only tackle the problem of the comparison of the two methods for the same one-way configuration and a given velocity field, we do not cover the topic of the evaluation of the computational cost purely devoted to the two-way coupling of the phases. It is clear that such a topic would be necessary, and we can envision that such a coupling will be very advantageous for the Eulerian method since the exchange of mass, momentum and heat for the Lagrangian approach have to be distributed to the various Eulerian nodes of the gaseous phase, due to heterogeneous descriptions. Besides, such a problem also results in a kind of numerical "diffusion" related to the Lagrangian approach. Even if speculative, such a statement allows to predict that in such a context, for two-way coupling, the Eulerian description will be far cheaper in terms of computational cost without leading to any level of oscillation once the mesh is coarsened. Such a statement is consistent with

the conclusions from [11].

6 Conclusion

In the present paper, we have presented the Eulerian multi-fluid modeling for the description of polydisperse evaporating spray in large vortical gaseous structures with its precise set of assumptions and related limitations.

We have proposed a clear physical interpretation of the mathematical assumptions underlying the modeling and, more specifically, of the mono-kinetic assumption on which the semi-kinetic model relies and which leads to the pressureless gas dynamics system of conservation equations for the transport in physical space in the multi-fluid model. Starting from simple 1D configurations, we have been able to clarify the physical origin of the singularities. Besides, it was shown that such a behavior is also associated with a singular behavior as far as the Williams spray equation is concerned at the kinetic level of description; it will require taking into account droplet collisions in situation when the global droplet density is high enough. Thus we have been able to characterize the range of Stokes numbers for which the multi-fluid model provides an accurate solution. Yet the proposed study has to be completed in the framework of unsteady gaseous velocity fields and two-way coupling. This work is in progress.

We have highlighted the origin of the formation of singularities in both velocity and droplet mass density in the multi-fluid model and, thus, we have been able to propose a robust numerical method which can cope with such singularities. Strictly speaking, the multi-fluid model should only be used in configuration where such singularities do not form. However, in many configurations, we still have high levels of droplet concentration and droplet mass density gradients and even at some isolated locations, some singularity can appear and the resulting model and simulations still be relevant at a global level. Such a statement is illustrated through the detailed study we have proposed for the Taylor-Green configuration and the frozen turbulent gaseous flow fields. Consequently it is important to be able to use a very robust numerical method such as the one proposed in this paper which can cope with the singularities and extreme droplet mass density and velocity gradients. Let us notice that the observed singularities are the same as the one appearing in the transport in physical space for the DQMOM approach (see [16] and references therein) and that the proposed method apply to the resulting systems of equations.

Then the Eulerian multi-fluid model has been validated and thoroughly compared to a finely discretized Lagrangian solver and second order convergence (except in the presence of too high density gradients) has been observed as

far as transport in physical space is concerned. For evaporating case, we have retrieved the first order in size phase space; new high order multi-fluid based techniques are here required and are being developed [28]. The key issue demonstrated in this paper is the ability of the Eulerian multi-fluid model to capture the size-conditioned dynamics of the spray. Such a property, proven in various test-cases, will be important for more complex configuration and combustion applications [9].

Finally, the two gas configurations allowed us to present a precise discussion about the computational efficiency of both descriptions for a given level of compared accuracy. The Taylor-Green configuration did not exhibit very different computational costs, due to the important simplifications arising from the analytical gas velocity field. Nevertheless it has been the occasion to develop a systematic procedure in order to compare two heterogeneous types of solvers and define comparable levels of precision on one Eulerian grid associated to the gaseous discretization. We have been able to conduct a precise study of the computational efficiency of the two methods at given accuracy. We have shown the reduced cost of the Eulerian solver as well as its ability to still provide non-oscillating solutions at low levels of accuracy even if the numerical diffusion can start to play a role in such a case. Furthermore, the Eulerian multi-fluid model can be parallelized, for example treating the different sections of the method with different processors, thus foreseeing significant improvement of the computational efficiency of the method. This accurate comparison between Eulerian and Lagrangian solvers has now to be extended to more complex configurations as 2D-axisymmetrical or 3D jets and is currently in progress.

Acknowlegments

The present research was done thanks to a Young Investigator Award from the French Ministry of Research (New Interfaces of Mathematics - M. Massot, 2003-2006), to the support of European Commission through the project "Towards Innovative Methods for Combustion Prediction in Aeronautic Engines" (TIMECOP-AE, project N : AST5-CT-2006-030828) and the support of an ANR (National Research Agency - France) Young Investigator Award (M. Massot, 2006-2009). The authors also acknowledge the support from IDRIS-CNRS (Institut de Developpement et de Ressources en Informatique Scientifique, Centre National de la Recherche Scientifique) where some of the computations were performed. The present work, conducted during the Ph.D. Thesis of S. de Chaisemartin (Laboratory EM2C - UPR CNRS 288), is supported by a grant from both DGA and CNRS and has received the support of the INCA project (National Initiative for Advanced Combustion) which is gratefully acknowledged.

References

[1] B. Abramzon and W.A. Sirignano. Droplet vaporization model for spray combustion calculations. *Int. J. Heat Mass Transfer*, 32:1605–1618, 1989.

[2] A.A. Amsden, P.J. O'Rourke, and T.D. Butler. Kiva ii, a computer program for chemically reactive flows with sprays. Technical Report LA-11560-MS, Los Alamos National Laboratory, 1989.

[3] E. Aulisa, S. Manservisi, R. Scardovelli, and S. Zaleski. A geometrical area-preserving volume-of-fluid method. *J. Comput. Phys.*, 192:355–364, 2003.

[4] G. A. Bird. Molecular gas dynamics and the direct simulation of gas flows. *Oxford Science Publications*, 42, 1994.

[5] F. Bouchut. On zero pressure gas dynamics. In *Advances in kinetic theory and computing*, pages 171–190. World Sci. Publishing, River Edge, NJ, 1994.

[6] F. Bouchut, S. Jin, and X. Li. Numerical approximations of pressureless and isothermal gas dynamics. *SIAM J. Num. Anal.*, 41:135–158, 2003.

[7] C. Cercignani, R. Illner, and M. Pulvirenti. *The mathematical theory of dilute gases*. Springer-Verlag, New York, 1994.

[8] S. Chapman and T. G. Cowling. *The mathematical theory of nonuniform gases*. Cambridge Mathematical Library. Cambridge University Press, Cambridge, third edition, 1990. An account of the kinetic theory of viscosity, thermal conduction and diffusion in gases, In co-operation with D. Burnett, With a foreword by Carlo Cercignani.

[9] S. de Chaisemartin, F. Laurent, L. Fréret, M. Massot, A-L. Birbaud, C. Lacour, S. Ducruix, and D. Durox. Pulsated free jets with spray injection : Eulerian Multi-Fluid modelling and simulation versus experimental measurements. In *Proceedings of the International Conference on Multiphase Flows, ICMF07, Leipzig*, 2007.

[10] S. Descombes and M. Massot. Operator splitting for nonlinear reaction-diffusion systems with an entropic structure: singular perturbation and order reduction. *Numer. Math.*, 97(4):667–698, 2004.

[11] O. A. Druzhinin and S. E. Elghobashi. A lagrangian-eulerian mapping solver for direct numerical simulation of bubble-laden turbulent shear flows using the two-fluid formulation. *J. Comput. Phys.*, 154:174–196, 1999.

[12] G. Dufour. *Modélisation multi-fluide eulérienne pour les écoulements diphasiques à inclusions dispersées*. PhD thesis, Université Paul Sabatier Toulouse III, 2005.

[13] G. Dufour and P. Villedieu. A second-order multi-fluid model for evaporating sprays. *M2AN Math. Model. Numer. Anal.*, 39(5):931–963, 2005.

[14] J. K. Dukowicz. A particle-fluid numerical model for liquid sprays. *J. Comput. Phys.*, 35(2):229–253, 1980.

[15] J. Dupays, Y. Fabignon, P. Villedieu, G. Lavergne, and J. L. Estivalezes. Some aspects of two-phase flows in solid-propellant rocket motors. In

Solid Propellant Chemistry, Combustion, and Motor Interior Ballistics, volume 185 of *Progress in Astronautics and Aeronautics*. AIAA, 2000.

[16] R. Fox, F. Laurent, and M. Massot. Numerical simulation of spray coalescence in an eulerian framework : direct quadrature method of moments and multi-fluid method. 2007. Submitted to Journal of Computational Physics, http://hal.archives-ouvertes.fr/hal-00157269.

[17] J.B. Greenberg, I. Silverman, and Y. Tambour. On the origin of spray sectional conservation equations. *Combustion and Flame*, 93:90–96, 1993.

[18] M. Herrmann. A Eulerian level set/vortex sheet method for two-phase interface dynamics. *J. Comput. Phys.*, 203(2):539–571, 2005.

[19] J. Hylkema. *Modélisation cinétique et simulation numérique d'un brouillard dense de gouttelettes. Application aux propulseurs à poudre*. PhD thesis, ENSAE, 1999.

[20] J. Hylkema and P. Villedieu. A random particle method to simulate coalescence phenomena in dense liquid sprays. In *Lecture Notes in Physics*, volume 515, pages 488–493, Arcachon, France, 1998. Proc. 16th Int. Conf. on Num. Meth. in Fluid Dyn.

[21] P.-E. Jabin. Various levels of models for aerosols. *Mathematical Models and Methods in Applied Sciences*, 12(7):903–919, 2002.

[22] C. Josserand, L. Lemoyne, R. Troeger, and S. Zaleski. Droplet impact on a dry surface: triggering the splash with a small obstacle. *Journal of fluid mechanics*, 524:47–56, 2005.

[23] F. Laurent. Numerical analysis of Eulerian multi-fluid models in the context of kinetic formulations for dilute evaporating sprays. *M2AN Math. Model. Numer. Anal.*, 40(3):431–468, 2006.

[24] F. Laurent and M. Massot. Multi-fluid modeling of laminar poly-dispersed spray flames: origin, assumptions and comparison of the sectional and sampling methods. *Comb. Theory and Modelling*, 5:537–572, 2001.

[25] F. Laurent, M. Massot, and P. Villedieu. Eulerian multi-fluid modeling for the numerical simulation of coalescence in polydisperse dense liquid sprays. *J. Comp. Phys.*, 194:505–543, 2004.

[26] R. J. LeVeque. *Finite volume methods for hyperbolic problems*. Cambridge Texts in Applied Mathematics. Cambridge University Press, Cambridge, 2002.

[27] D. L. Marchisio and R. O. Fox. Solution of population balance equations using the direct quadrature method of moments. *Journal of Aerosol Science*, 36:43–73, 2005.

[28] M. Massot, F. Laurent, and D. Kah. Moment methods for population balance equations describing polydisperse evaporating sprays : the key issue of evaluating the flux of disappearing droplets. *Journal of Aerosol Science*, 2007. submitted for publication.

[29] R. S. Miller and J. Bellan. Direct numerical simulation of a confined three-dimensional gas mixing layer with one evaporating hydrocarbon-droplet-laden stream. *Journal of Fluids Mechanics*, 384:293–338, 1999.

[30] R. S. Miller and J. Bellan. Direct numerical simulation and subgrid anal-

ysis of a transitional droplet laden mixing layer. *Phys. Fluid*, 12(3):650–671, 2000.

[31] P. J. O'Rourke. *Collective drop effects on vaporizing liquid sprays*. PhD thesis, Princeton University, 1981.

[32] J. Reveillon and F.X. Demoulin. Effects of the preferential segregation of droplets on evaporation and turbulent mixing. *J. Fluid Mech., accepted for publication*, 2007.

[33] J. Reveillon, C. Péra, M. Massot, and R. Knikker. Eulerian analysis of the dispersion of evaporating polydispersed sprays in a statistically stationary turbulent flow. *Journal of Turbulence*, 5(1):1–27, 2004.

[34] M. Rüger, S. Hohmann, M. Sommerfeld, and G. Kohnen. Euler/Lagrange calculations of turbulent sprays: the effect of droplet collisions and coalescence. *Atomization and Sprays*, 10(1):47–81, 2000.

[35] S. Tanguy and A. Berlemont. Development of a level set method for interface tracking: application to droplet collisions. *International Journal of Multiphase Flows*, 31(9):1015–1035, 2005.

[36] Y. Tsuji, T. Tanaka, and S. Yonemura. Cluster patterns in circulating fluidized beds predicted by numerical simulation (discrete particle versus two-fluid models). *Powder Technology*, 95:254–264, 1998.

[37] A.N. Volkov, Yu.M. Tsirkunov, and B. Oesterl. Numerical simulation of a supersonic gas-solid flow over a blunt body : The role of inter-particle collisions and two-way coupling effects. *International journal of multiphase flow*, 31(12):1244–1275, 2005.

[38] F. A. Williams. Spray combustion and atomization. *Phys. Fluids*, 1:541–545, 1958.

[39] F. A. Williams. *Combustion Theory (Combustion Science and Engineering Series)*. ed F A Williams (Reading, MA: Addison-Wesley), 1985.

[40] Ya. B Zel′dovich. Gravitational instability : an approximate theory for large density perturbations. *Astronomy and Astrophysics*, 5:84–89, 1970.